https://doi.org/10.5194/egusphere-2026-3521
Preprint. Discussion started: 3 August 2026

FireLands 1.0: A landscape evolution model for simulating the effects of fires and post-fire erosion on sediment dynamics in evolving landscapes

Matheus de Almeida[1,2], Charles M. Shobe[3], Duna C. Roda-Boluda[2,4], Loraine Gourbet[1], Amber Distelbrink[1,2], Sander Veraverbeke[2,5], and Benjamin Campforts[2]

[1]GFZ Helmholtz Centre for Geosciences, Potsdam, Germany
[2]Department of Earth Sciences, Vrije Universiteit Amsterdam, Amsterdam, Netherlands
[3]U.S. Forest Service Rocky Mountain Research Station, Fort Collins, CO, United States
[4]Geology Department, Universitat Autonoma de Barcelona, Barcelona, Spain
[5]School of Environmental Sciences, University of East Anglia, Norwich, United Kingdom

Correspondence: Matheus de Almeida (m.wanderleydealmeida@vu.nl)

Abstract.

Wildfires play an important control on changing Earth surface processes across a wide range of landscapes. Although post-fire changes in erosion and deposition dynamics have been widely documented, feedbacks among wildfire, vegetation, sediment dynamics, and topographic adjustment across large temporal and spatial scales remain poorly understood. Landscape evolution models provide a powerful framework for integrating these processes and timescales, enabling assessment of how wildfire influences long-term landscape evolution. Here, we present FireLands, a landscape evolution model that integrates a newly developed component for fire ignition and spread (*WildfireGenerator*) with existing components for landscape evolution processes. *WildfireGenerator* is a cellular automaton model simulating fire ignition and spread, aridity-controlled fire severity and vegetation regrowth. Within FireLands, *WildfireGenerator* is coupled with components for soil production, erosion by channelized flow, and hillslope sediment transport. We link wildfire effects to geomorphic process efficiency by positing fire-driven increases in sediment erodibility and hillslope transport efficiency, with the highest increases occurring after high-severity fires. Model testing suggests that WildfireGenerator realistically simulates the effects of fire on vegetation and the emergence of landscape-scale vegetation patterns. An observed fire magnitude–frequency relationship from Calabria, a wildfire-prone region in southern Italy, is reproduced with good agreement. Simulations incorporating coupling between wildfire and landscape evolution show that FireLands captures key aspects of post-wildfire geomorphic response, whereby vegetation controls the magnitude of erosion on hillslopes and deposition within higher-order fluvial channels. The magnitude and spatial extent of sediment redistribution across post-fire landscapes depend on fire frequency and severity, vegetation recovery rates and landscape heterogeneity. FireLands is able to simulate these dynamics across large spatial and temporal scales, providing a tool for integrating short-duration, high-intensity geomorphic extremes driven by wildfire within a long-term landscape evolution framework. Including fires in a landscape evolution perspective is powerful to understand the effects of fire-vegetation feedbacks on sediment transport over various spatial and temporal scales.

https://doi.org/10.5194/egusphere-2026-3521
Preprint. Discussion started: 3 August 2026

1 Introduction

Fires are important hydrological and geomorphological agents (Shakesby and Doerr, 2006). Fires cause a combination of ground-cover removal and increased temperature in the topsoil, which result in decreased root strength, soil cohesion and infiltration capacity, therefore increasing soil erodibility and sediment yield (Doerr et al., 2025; Sousa et al., 2026). Post-fire erosion rates can be several orders of magnitude higher than background erosion rates. Considering geological timescales, post-fire erosion can contribute meaningfully to long-term erosion rates (10^6 years). For example, in the western United States, fire-related erosion accounts for at least 25% of long-term values, which can increase up to 80% depending on topography and fire return interval (Roering and Gerber, 2005). In the continental United States, erosion related to moderate and high severity fires may contribute up to 90% of total erosion on geological timescales (Orem and Pelletier, 2016).

The removal of vegetation is one of the biggest changes in the land surface after a fire, which enhances the occurrence of surface processes such as rill erosion, gullying, shallow landslides, and debris flows (see Rengers and Mcguire (2021) and McGuire et al. (2024)). In steep landscapes, fire also potentiates dry-ravel processes, which are a major driver of post-fire sediment transport (Jackson and Roering, 2009; Guilinger et al., 2023). Although increased fire-induced erosion rates are temporary, they can persist for decades if multiple fires are considered (Vieira et al., 2026). This increase is variable and can be controlled by vegetation recovery, the development of surface lag deposits (Rengers et al., 2016), soil production (Roering and Gerber, 2005) and sediment availability (Noske et al., 2024; Ryan et al., 2024).

There is a reasonably good understanding on the geomorphic effects of fires in the years or decades post-fire (Rengers et al., 2016; McGuire et al., 2024; Rengers et al., 2026). Some studies have also quantified long-term post-fire erosion (e.g. Orem and Pelletier, 2016; Rengers et al., 2021), yet the effects of fires on landscape evolution and sediment redistribution remain difficult to quantify due to our limited observational timescale. This limitation can be overcome by using numerical models, which have proven useful to explain landforms, their feedback mechanisms, and rates of change over various temporal and spatial scales (Tucker and Hancock, 2010). There are two categories of numerical models for Earth surface processes that have been used to assess post-fire erosion. A first category consists of soil erosion models. These models are often calibrated with post-fire data to estimate fire-induced erosion (e.g. Larsen and MacDonald, 2007; Karamesouti et al., 2016; Bircher et al., 2022). The most widely used models to estimate post-fire erosion are Revised Universal Soil Loss Equation, RUSLE, (Renard et al., 1991; Vieira et al., 2026) and Water Erosion Prediction Project, WEPP, (Flanagan and Nearing, 1995; Dow et al., 2024), among others (e.g. Pan–European Soil Erosion Risk Assessment, PESERA, Kirkby et al. (2008)), providing valuable information on post-fire sediment transport over the past decades. However, the erosion models currently used do not cover the necessary temporal and spatial scales to understand post-fire landscape recovery feedbacks (e.g. post-fire increase in erosion followed by a decay due to recovery of soil properties and vegetation) and the effects of soil production and hillslope processes on sustaining soil-mantled landscapes. The lack of consideration of sediment availability and soil production, for example, may result in overestimated modeled post-fire erosion rates, especially in areas with shallow soils.

A second category of models is Landscape Evolution Models (LEMs). LEMs are numerical models useful for simulating the interactions among climate, tectonics, and erosion over various temporal and spatial scales (Tucker and Hancock, 2010)

https://doi.org/10.5194/egusphere-2026-3521
Preprint. Discussion started: 3 August 2026

and enable simulation of stochastic events and their influence on sediment dynamics (e.g. landslides (Campforts et al., 2020)). One of the biggest advantages of a LEM is the capability of combining a statement of continuity of mass with different geomorphic processes equations (e.g. channel erosion, soil production and hillslope processes) over up to 10^6 year timescales (Tucker and Hancock, 2010). A LEM framework is capable of dynamically coupling other models of Earth natural processes, such as individual storms (Shmilovitz et al., 2025) or fires, interacting with geomorphic components. Although LEMs are potentially powerful tools for post-fire erosion assessments, few studies have implemented LEMs in fire prone landscapes. Roering and Gerber (2005) showed that fire-related sediment fluxes increase with more frequent fires. Istanbulluoglu and Bras (2005) used a LEM to understand the effects of vegetation on sediment yields and showed that wildfires are responsible for increasing drainage density and decreasing topographic relief. However, both studies did not simulate sediment deposition through channel processes, which is an important aspect to understand river aggradation in fire-prone landscapes (Santi and Rengers, 2020).

Given the impact fire has on Earth surface, fire models have been widely used to understand fire dynamics on various spatial scales. There are two important types of fire models. The first are global fire models, which simulate the long-term fire occurrence based on climate, vegetation and human activity (Hantson et al., 2016). Global fire models are capable of simulating climate-vegetation feedbacks governing fire activity on coarse spatial scales (see review Hantson et al., 2016). The second type is landscape level fire models. These models simulate fire ignition and growth as a result of weather (such as wind-driven fire spread), topography (elevation, aspect, slope) and vegetation (e.g. Rothermel, 1972; Finney, 2006). To understand how climate-controlled fuel availability drives fire activity at landscape level, it becomes necessary to combine the characteristics of both global and landscape scale fire models. To do this, we aim to develop a fire model capable of simulating long-term fire regimes based on vegetation-climate feedbacks (global fire model) controlling short-term fire spread based on topography and vegetation (landscape-level model). Then it becomes possible to integrate both long and short term fire effects in a LEM framework.

Here, we present FireLands, a new LEM built by integrating a newly developed fire component with existing components for sediment transport and soil production from bedrock. FireLands is capable of simulating the feedback mechanisms between fire, vegetation, sediment dynamics, and topography. By coupling a fire model into a LEM framework, we aim to better understand post-fire landscape recovery, sediment storage, and soil sustainability over various temporal and spatial scales. For the fire model component, we designed *WildfireGenerator*, a cellular automata model that uses a climate-fire relationship to dynamically simulate fire ignition, spread, severity and vegetation recovery. *WildfireGenerator* is built within Landlab framework (Hobley et al., 2017; Barnhart et al., 2020), enabling the combination with geomorphic components already available in Landlab. In this paper, we describe *WildfireGenerator* and how it is integrated with process-based erosion and deposition models in a LEM framework. We evaluate the ability of *WildfireGenerator* to represent theoretical climate-fire relationships and generate realistic vegetation patterns under different fire regimes. Next, we simulate the impact of fires on synthetically evolving topography using the coupled FireLands model. Finally, we discuss model limitations and potential calibration strategies.

https://doi.org/10.5194/egusphere-2026-3521
Preprint. Discussion started: 3 August 2026

2 Fire behaviour and post-fire erosion

2.1 Fire regimes and its drivers

Fire regimes can be defined as the long-term patterns in fire frequency, severity, size and spatial distribution in a given region (Morgan et al., 2001; Scholten et al., 2024). In this paper, fire severity is defined as the short-term fire effects measured immediately post-fire (Veraverbeke et al., 2010), and fire size is the total burned area covered by a single fire. Fire regimes are primarily controlled by fuel availability, weather conditions (Moritz et al., 2005), and number of fire ignitions per time period (Archibald et al., 2009; Bradstock, 2010; Krawchuk and Moritz, 2011). Fuel availability, defined as the amount of organic material above ground, and moisture, commonly inferred from aridity (Pausas and Bradstock, 2007), together regulate how much material is prone to burning (Bradstock, 2010). Aridity is determined by the level of atmospheric dryness, often measured with vapor pressure deficit (VPD) as a proxy (Anderson, 1936; Yuan et al., 2019). While low aridity represents humid and high productivity environments, high aridity regions are marked by their dryness, with limited productivity and vegetation growth (Sanginés de Cárcer et al., 2018; Yuan et al., 2019). Fire regimes are influenced by aridity through several mechanisms. Aridity plays an important role controlling the spatial patterns of fire activity (Sedano and Randerson, 2014; Chen et al., 2021; Cardoso et al., 2022), and is associated with an expansion of high-severity burned areas for different biomes (Grünig et al., 2023; Parks et al., 2025). Therefore, the projected alterations in aridity for the next decades can be a useful indicator to predict changes in fire activity (Abram et al., 2021; Parks et al., 2025).

The existing relationship between aridity and fuel availability is the basis for a theoretical model (Figure 1) that represents how fire regimes vary as a function of aridity. This theoretical model is described as a humped relationship, where fire activity is low in humid, low aridity regions, peaks under intermediate aridity and decreases in dry, arid regions (see Pausas and Ribeiro, 2013). In areas where aridity is low and vegetation is dense (high productivity), fuel availability does not impose a limitation on fire activity, and increasing aridity is translated into an increase in fire frequency (Pausas and Bradstock, 2007). In contrast, fire activity in arid regions is limited by low fuel availability in the landscape (due to low productivity) (Pausas and Bradstock, 2007; Kampf et al., 2025). Fire activity is expected to peak in areas of intermediate aridity (Pausas and Bradstock, 2007; Bradstock, 2010; Kampf et al., 2025), where aridity is high enough to promote frequent fire ignition and growth, but where vegetation is still dense enough to not yet impose a limitation to burning. The fire activity-aridity relationship described in Figure 1 has been validated in regions of temperate (Kampf et al., 2025) and mediterranean (Pausas and Bradstock, 2007; Pausas and Paula, 2012) climates, and serve as basis for a global fire-aridity relationship (Pausas and Ribeiro, 2013).

2.2 Post-fire geomorphic response

The occurrence of post-fire geomorphic processes may increase erosion rates by several orders of magnitude. The magnitude of post-fire erosion rate perturbations varies depending on the spatial and temporal scales of analysis. At a hillslope plot scale, post-fire erosion rates can increase by two orders of magnitude relative to unburned hillslopes (e.g., Benavides-Solorio and MacDonald, 2001; Larsen et al., 2009; Abrahams et al., 2018; Vieira et al., 2018). In burned catchments, measured ^{10}Be-derived catchment-average erosion rates can show an increase of up to 3 orders of magnitude higher than in unburned catchments

https://doi.org/10.5194/egusphere-2026-3521
Preprint. Discussion started: 3 August 2026

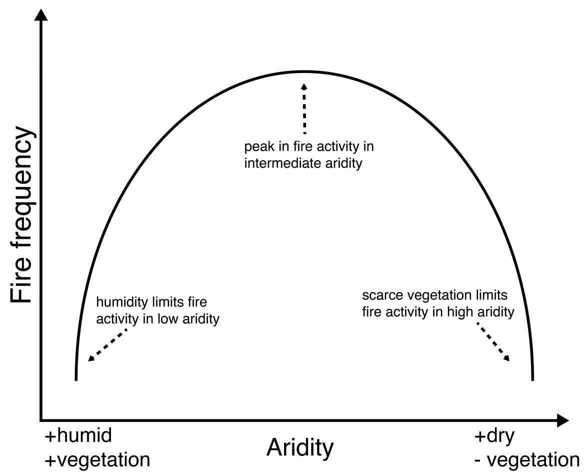

Figure 1. (a) Conceptual relationship between fire frequency and aridity, modified from Pausas and Bradstock (2007) and Bradstock (2010). At low aridity, vegetation is abundant, and humidity limits fire frequency due to the higher amount of moisture available in the atmosphere. There is a peak in fire frequency at intermediate levels of aridity, where humidity and fuel availability equally control fire ignition. Fire frequency decays at high aridity, as the lack of vegetation becomes a limitation for fire ignition.

(Orem and Pelletier, 2016). Currently, post-fire erosion represents ca. 20% of the global soil erosion budget, and based on future climate projections, post-fire erosion is predicted to increase ca. 30% by 2070 (Vieira et al., 2026).

The removal of vegetation cover and increase in soil exposure caused by fires can induce (or enhance) the occurrence of several geomorphic processes. Rill and interrill erosion, gullying, shallow landslides, and debris flow are processes often triggered after fires and contribute to increase sediment transport on various spatial and temporal scales (see reviews of Moody et al. (2013), McGuire et al. (2024)). Rill and interrill are water erosion processes that occur when sediment particles are detached from the land surface by raindrops and transported by overland flow (Kinnell, 2005). Additionally, the sediment mobilized by overland flow can increase the volume of post-fire debris-flows (Alessio et al., 2021). Dry ravel, the process of downslope movement of sediment by gravity (Rice, 1982), is a major source of post-fire hillslope sediment in steep landscapes, as the removal of vegetation releases trapped sediment. The material mobilized by dry-ravel processes is transported from steep hillslopes, and deposited in areas where slopes are lower than the angle of repose and along the valley floor (Lamb et al., 2011; DiBiase and Lamb, 2019).

The increase in post-fire erosion also depends on landscape characteristics, such as lithology, topography, climate, soil properties, and catchment area (Santi and Rengers, 2020; McGuire et al., 2024). In low-order catchments (drainage area $\leq$ 10 km^2), sediment evacuation is influenced by the degree of connectivity between hillslopes and fluvial channels, so that hillslope-derived sediment reaches the trunk streams through rill, interrill, and mass wasting processes. In high-order catchments (drainage area $\geq$ 10 km^2), the increase in sediment evacuation depends on the amount of material supplied from low-order catchments and adjacent hillslopes (McGuire et al., 2024).

https://doi.org/10.5194/egusphere-2026-3521
Preprint. Discussion started: 3 August 2026

Understanding the drivers of sediment mobilization after the fire is also critical to increasing our knowledge of longer term fire-related sediment dynamics. After the post-fire erosion increase, vegetation starts to recover, re-establishing soil cohesion, and erosion rates return to the average long-term base level (Cerdà, 1998; Inbar et al., 1998; Benavides-Solorio and MacDonald, 2005). This period of increase and decay in sediment transport is described as the fire "window of disturbance", and has been observed to range between 1-7 years typically (Santi and Rengers, 2020). The post-fire sediment cascade during the window of disturbance is influenced by several factors, such as sediment availability, fire characteristics, time since the last fire, topography, climate and vegetation (Moody et al., 2013; Noske et al., 2024; McGuire et al., 2024). The post-fire vegetation recovery rate sets the pace of ground cover reestablishment, which stabilizes the soil and decreases sediment transport over time (Cerdà, 1998; Benavides-Solorio and MacDonald, 2005), and therefore influences the period in which the window of disturbance is active. Sediment availability may also control the magnitude of the window of disturbance, as the increase in erosion rates can be curtailed by limitations in sediment supply (Ryan et al., 2024), which can vary with aridity (Noske et al., 2024). Regarding fire characteristics, fire severity is one of the most important controls on post-fire erosion (Benavides-Solorio and MacDonald, 2005; Shakesby and Doerr, 2006). Moreover, the concept of window of disturbance was proposed looking after a single fire event, whereas regions frequently affected by fires experience the effect of cumulative fires, which may increase average base level erosion rates not only for 1-7 years, but for several decades (Vieira et al., 2026). This is the case for many fire-prone landscapes, where most of the areas have already burned at least once and are in a stage of response to the fire event (e.g. Thomas et al., 2025).

3 Model description

FireLands is a LEM capable of simulating landscape response to fire dynamics. FireLands is built by combining a newly developed Landlab fire component (*WildfireGenerator*) with existing erosion and deposition components (Figure 2). *WildfireGenerator* is a cellular automaton that simulates fire regimes based on climate-vegetation interactions. Following a fire, hillslope soil transport and water erosion processes are enhanced in response to reduced vegetation, with the highest increases occurring after high severity fires. Thus, there is an increase in sediment erodibility (for water erosion processes) and transport efficiency (for hillslope sediment transport) following each fire. Sediment erodibility and hillslope transport efficiency then start to decay as vegetation recovers and soil ground cover increases with time. The duration and magnitude of the window of disturbance are controlled not only by vegetation recovery but also by geomorphic and geologic constraints such as soil thickness and production.

3.1 A cellular wildfire automaton

WildfireGenerator is a landscape-scale cellular automata (CA) model based on long-term fuel-climate dynamics. CAs are mathematical idealizations of physical systems in which space and time are discrete and consist of a regular array of cells, each containing a discrete variable (Wolfram, 1994). What distinguishes CAs from other mathematical models is the set of algorithms (or rules) that drive the interactions among cells, which are always local, between a cell and its neighbour. In this

https://doi.org/10.5194/egusphere-2026-3521
Preprint. Discussion started: 3 August 2026

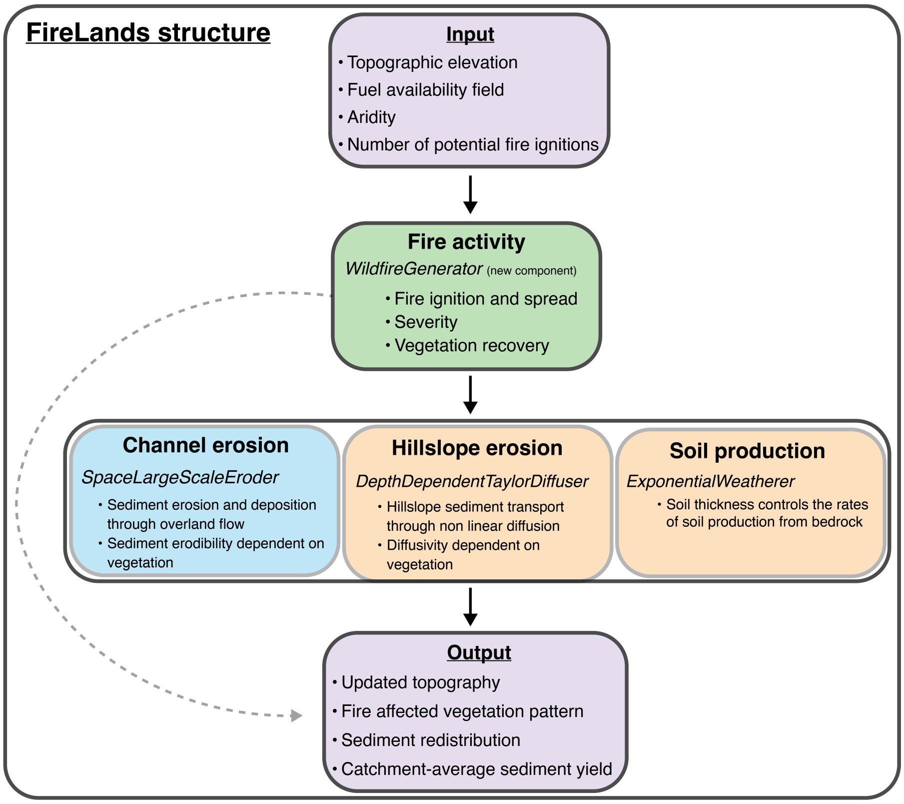

Figure 2. Diagram overview of FireLands inputs, coupled components, and outputs. FireLands couples the newly developed *WildfireGenerator* component with already available models for channel and hillslope erosion, and soil production. FireLands outputs the updated topography, vegetation, sediment thickness and sediment yield controlled by climate-fire interactions. *WildfireGenerator* can also be instantiated alone, only updating the vegetation field (dashed line).

case, at each time step, a cell's variable is updated based on the values of that same variable in a neighbour cell, following the defined set of rules (Wolfram, 1994). CA models are useful tools for understanding fire dynamics and provide valuable information for fire prevention (Freire and DaCamara, 2018), as they are computationally efficient in simulating the behavior of complex physical mechanisms (Toffoli, 1984). Fire behavior models have been widely developed in recent decades, and several of them use cellular automata to efficiently simulate fire spread in a landscape and understand the controls on fire susceptibility (e.g. Pais et al., 2021; Zhou et al., 2025).

The *WildfireGenerator* rules for fire initiation and growth are based on fuel availability and aridity, which together determine the amount of dry fuel available to burn. In the current version of *WildfireGenerator*, we assume that fire ignitions occur randomly in space and time. However, there are specific landscape characteristics, such as the presence of large rivers that act as firebreaks, where fires are not allowed to ignite or spread.

https://doi.org/10.5194/egusphere-2026-3521
Preprint. Discussion started: 3 August 2026

3.1.1 Fire ignition

Fire ignition (P_i) is implemented following Pausas and Ribeiro (2013), and is controlled by two normalized dimensionless indices: fuel availability (f_a) and aridity (a) (Eq 1). aridity (a) varies from 0 (non-arid, wet) to 1 (arid, dry), does not vary spatially and is used to represent levels of atmospheric dryness. a_w and f_w are weights that determine the relative control of aridity (a) and fuel availability (f_a), respectively, on the probability of a fire to start.

$$P_i = f_a\ f_w + a\ a_w \tag{1}$$

f_a is spatially variable in the domain and represents the value of fuel availability in the landscape, ranging from 0 to 1. While $f_a = 0$ means that the soil is completely exposed, without vegetation above its surface, $f_a = 1$ represents the maximum value of fuel availability. For fire regimes where vegetation is scarce and limits fire activity (right section of Figure 1), must have a higher value than a_w, which means that vegetation has a bigger importance in controlling the probability of fire ignition (see Kampf et al. (2025)). Conversely, to represent regions where vegetation is not a limitation and fires depend on vegetation dryness (left section of Figure 1), a_w must be equal or higher than f_w, so that aridity becomes the main control on the probability of fire ignition. In this model, a_w and f_w are equal to 0.5 for all aridity values between 0 and 0.5. In that case, fire ignition is sensitive to changes in aridity (as proposed by Pausas and Ribeiro (2013)). As aridity increases to higher than 0.5, vegetation becomes the main limitation for fire ignition, and the fuel availability variable is the main controller of the probability for ignition. We set $f_w = 0.8$ and $a_w = 0.2$ when aridity ranges between 0.5 and 0.7, and $f_w = 0.9$ and $a_w = 0.1$ if aridity is higher than 0.7.

3.1.2 Fire spread

Fire spread is simulated based on the concept of Pausas and Paula (2012), where the fuel-climate relationship is the main driver of vegetation connectivity, allowing fires to spread. Here, fire spread (P_s) is controlled by fuel availability, aridity, and slope.

$$P_s = (f_a\ f_w + a\ a_w)\ \ S_f \tag{2}$$

where

$$S_f = \frac{1}{1 + \exp(-\alpha\ \frac{\Delta z}{\Delta x})} \tag{3}$$

Similarly to Eq. 1, the probability of fire spread is influenced by the interaction between f_a and a as prescribed by values for a_w and f_w. Fires tend to spread upslope due to convective heat transfer (Rothermel, 1972; Liu et al., 2014). Here, we apply a slope factor S_f (Eq. 3), which accounts for slope differences ($\frac{\Delta z}{\Delta x}$), by applying a scaling factor α of 0.3. This value is used here to create a preference for the upslope spreading of the fire (when $\frac{\Delta z}{\Delta x} > 0$). As α increases, the model sets a higher preference for the upslope spread of fires. Equation 3 outputs a value ranging from 0 to 1, creating a bias in P_s and the upslope areas become more likely to burn.

https://doi.org/10.5194/egusphere-2026-3521
Preprint. Discussion started: 3 August 2026

3.1.3 Fire severity

Fire severity (F_s) is estimated by the power law relationship proposed by Grünig et al. (2023) (Figure 3) in which severity increases with aridity. As aridity decreases, fires become less severe due to increased moisture (Eq. 4).

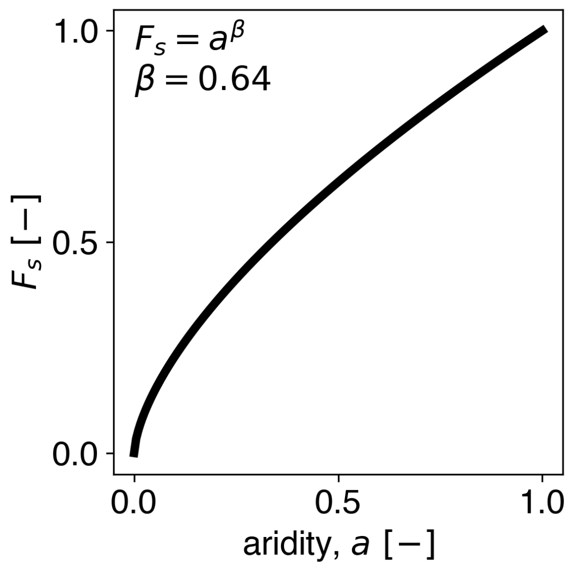

Figure 3. Power-law relationship between fire severity (F_s) and aridity (a) based on the correlation between a satellite-derived proxy of fire severity, and summer vapour pressure deficit (VPD), a proxy of aridity (Grünig et al., 2023). The power-law exponent (β) of 0.64 represents the best fit for the Mediterranean biome, and its value varies for different biomes (see Grünig et al. (2023) for more details).

$$F_s = a^\beta \quad (4)$$

F_s is the dimensionless severity index simulated for each fire and β is the exponent of the power law relationship. F_s ranges from 0 to 1 and determines the proportion of vegetation removed after a fire (Eq. 5), where 1 represents a fire with the highest severity, completely removing the vegetation, and 0.1 represents one of the lowest severities, burning only 10% of the vegetation. Empirical values of β were proposed by Grünig et al. (2023) and range from 0.17 to 0.64, depending on the climate-vegetation interactions of different biomes. In Eq. 5, $f_{a_{post}}$ is the fuel availability left after a fire and $f_{a_{pre}}$ is the value of fuel availability before the fire.

$$f_{a_{post}} = (1 - F_s) f_{a_{pre}} \quad (5)$$

https://doi.org/10.5194/egusphere-2026-3521
Preprint. Discussion started: 3 August 2026

3.1.4 Vegetation recovery

After a fire occurs, the vegetation starts to recover. Viedma et al. (1997) calibrated a vegetation recovery rate model using satellite data from a landscape with sparse shrubs, dense shrubs, and trees mixed with shrubs. Gouveia et al. (2010) proposed a similar monoparametric vegetation recovery model using monthly NDVI (Normalized Difference Vegetation Index) values. For this framework, we used the model proposed by Viedma et al. (1997) as it is calibrated in a yearly time interval, which matches the timestep defined in the simulations for this work. (Eq. 6).

$$f_a(t) = 1 - \exp(-r t_r) \tag{6}$$

Vegetation recovery varies as a function of the total recovery time t_r [T] and the regrowth exponent r [T^{-1}], which controls the rate of f_a regrowth. High r means that vegetation recovers to stability in a shorter period of time compared to low r, where vegetation goes through a slower recovery process (Viedma et al., 1997). For example, Mediterranean shrublands show t_r ranging from 5.4 to 18.5 years to reach a recovery of 90% after a fire, with a fitted r associated for every t_r (Table 1) (Viedma et al., 1997). Vegetation type also changes with the total recovery time t_r. As t_r increases, the vegetation type can change from "Trees + shrubs" to "Dense shrubs" and "Sparse shrubs" (Table 1). In *WildfireGenerator*, discrete values of both t_r and r are defined over prescribed aridity intervals and represent different vegetation types as reported in Table 1. Generally, t_r increases with aridity while r decreases with aridity. Therefore, it takes more time (higher t_r, lower r) to recover to pre-fire fuel availability in dry landscapes and less time to recover in wet landscapes.

Table 1. Post-fire vegetation recovery parameters as a function of aridity a. The total recovery time t_r increases with aridity a, and the vegetation type can change from "Trees + shrubs" to "Dense shrubs" and "Sparse shrubs".

Aridity (a)	**Total recovery time** (t_r)*	**Regrowth exponent** (r)*	**Vegetation type***
$0 \leq a < 0.1$	5.4	0.42	Trees + shrubs
$0.1 \leq a < 0.3$	8	0.29	Dense shrubs
$0.3 \leq a < 0.5$	12.4	0.18	Dense shrubs
$0.5 \leq a < 0.7$	15	0.15	Sparse shrubs
$0.7 \leq a < 1.0$	18.5	0.12	Sparse shrubs

* Values calculated by Viedma et al. (1997), for Mediterranean shrublands

3.2 Post-fire erosional response

The increase in post-fire sediment yield is primarily controlled by the loss of surface cover, overland flow and raindrop erosion. As vegetation recovers with time, erosion decreases to levels of undisturbed landscapes (Benavides-Solorio and MacDonald, 2005; Larsen et al., 2009). Therefore, we assume that fluvial sediment erodibility (K_{sed}) and hillslope transport efficiency (D)

https://doi.org/10.5194/egusphere-2026-3521
Preprint. Discussion started: 3 August 2026

increase after a fire with a magnitude proportional to the amount of vegetation loss. Erosion parameters increase exponentially with decreasing fuel availability f_a (Eqs. 7 and 8) as follows:

$$K_{sed} = K_{sed_0} k_{boost}{}^{(1-f_a)} \tag{7}$$

and

$$D = D_0 d_{boost}{}^{(1-f_a)} \tag{8}$$

where sediment erodibility K_{sed} (in Eq. 7) and diffusivity D (in Eq. 8) are controlled by f_a, and the boost factors k_{boost} and d_{boost} are the maximum increases in K_{sed} and D, respectively, after a fire. Equations. 7 and 8 follow the exponential relationship between sediment transport and percentage of bare soil (or lack of ground cover) measured by Larsen et al. (2009). For changes in erodibility, k_{boost} can vary, with an increase of up to 10^2 Nyman et al. (2013). For changes in diffusivity, the recorded post-fire increase in diffusivity is between 1 and 10 (Roering and Gerber, 2005), and can be used to parameterize d_{boost}.

The exponential relationship between fuel availability and erosion parameters (Eqs. 7 and 8) functions in a way that, for fires removing up to 40% of fuel availability, the erosion parameters do not increase substantially. However, as fire severity intensifies and more than 60% of vegetation is consumed, sediment transport increases exponentially until it reaches the maximum increase for fires that remove all vegetation (k_{boost} and d_{boost}) (Figure 4). After a post-fire increase in sediment erodibility K_{sed} and diffusivity D, they start to decay to their pre-fire values (K_{sed_0} and D_0, respectively) as vegetation f_a recovers to its maximum.

Aridity is a primary control for vegetation recovery (Sanginés de Cárcer et al., 2018; Yuan et al., 2019), which influences how long the post-fire enhanced erosion lasts (Vieira et al., 2026). Figure 5 shows how aridity controls the trajectory of post-fire changes in erodibility and diffusivity after the highest severity fire, which generates the biggest increase in erosion. We used $a = 0.09$ to represent the changes in erosion under low aridity, $a = 0.5$ for intermediate aridity, and $a = 1.0$ for high aridity conditions. The fastest decay in erosion parameters was found under low aridity, as it has an efficient post-fire vegetation recovery (Table 1). As aridity increases, vegetation recovery becomes slower, resulting in sustained periods of post-fire increased erodibility K_{sed} and diffusivity D.

4 Numerical implementation

4.1 *WildfireGenerator*: Vegetation and climate driving fire activity

WildfireGenerator simulates fire regimes by the interaction between fuel availability and aridity, keeping track of fire characteristics such as frequency, size, and severity. This code implements a spatially explicit cellular fire automaton in which each grid cell follows local, probabilistic ignition, spread, burning, and regrowth rules based on neighboring cell states (vegetation,

https://doi.org/10.5194/egusphere-2026-3521
Preprint. Discussion started: 3 August 2026

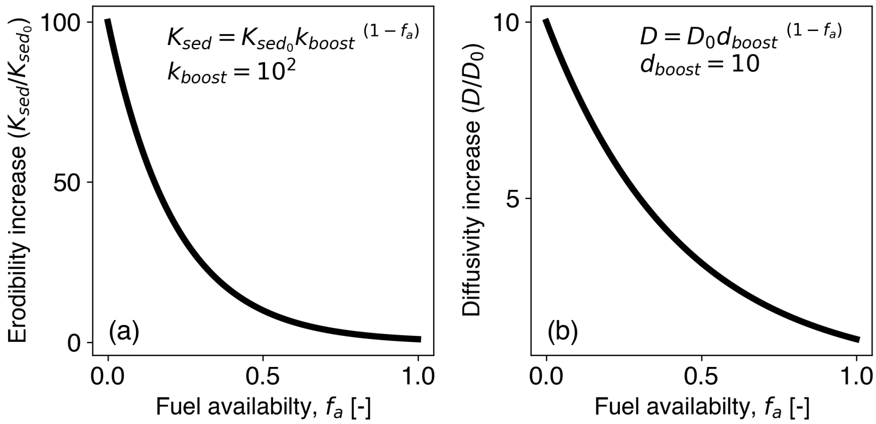

Figure 4. Changes in (a) sediment erodibility K_{sed} and (b) diffusivity D as a function of fuel availability f_a. Removal of vegetation by fire is connected with increases in erosion, since the percentage of bare soil increases (Benavides-Solorio and MacDonald, 2005; Larsen et al., 2009). Values of k_{boost} and d_{boost} are within the range of post-fire increase in erodibility (Nyman et al., 2013; McGuire et al., 2024) and diffusivity (Roering and Gerber, 2005), respectively.

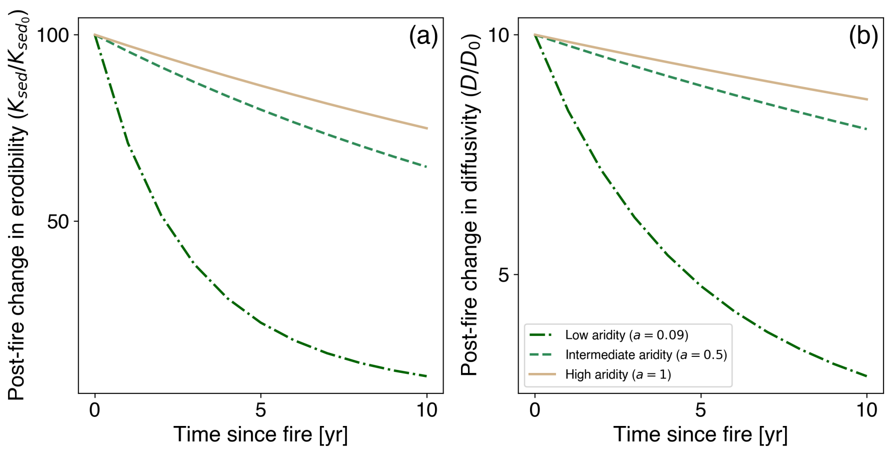

Figure 5. Post-fire changes in the erosion parameters (a) sediment erodibility and (b) diffusivity as a function of aridity, and time since the highest fire severity, where the vegetation is completely removed and erosion enhancement is at its maximum. Since vegetation recovery is faster at low aridity, it takes less time for erodibility and diffusivity to return to their initial values, K_{sed_0} and D_0, respectively.

aridity, slope, and firebreaks), producing emergent fire regimes at the landscape scale. In the current version, the *WildfireGenerator* simulates multiple fire occurrences in a yearly timestep, assuming that fires are triggered during the fire season (usually during summer), and wind, oxygen levels and heat are constant for fire activity. Although slope is accounted for fire growth, aspect and elevation do not play a role in fire activity. *WildfireGenerator* is developed in Landlab, an open source toolkit for

https://doi.org/10.5194/egusphere-2026-3521
Preprint. Discussion started: 3 August 2026

modeling Earth surface dynamics that facilitates the integration of new modules with existing landscape evolution components in a gridding engine (Hobley et al., 2017; Barnhart et al., 2020).

The *WildfireGenerator* starts with a number of potential fire ignitions randomly placed on a raster grid. Based on this number, *WildfireGenerator* defines the number of possible ignitions at every time step by drawing a sample from a Poisson distribution. The probability of fire ignition (Eq. 1) is calculated based on the values of fuel availability f_a and aridity a for every cell. A random number u [0,1] is generated and a fire ignites when u is smaller than P_i at the potential ignition cell, shifting the cell state from "unburned" to "burned" (Figure 6a).

After a fire ignites in a cell, it can spread to its orthogonal neighbors (Figure 6b-c). For every potential spread cell, the *WildfireGenerator* calculates the probability for fire spread based on their values of fuel availability, aridity, and slope (Eq. 2). A random number u [0,1] is generated and the fire spreads when u is smaller than P_s (Figure 6b). If the fire spreads to one (or more) neighbors, the neighbor cell changes its state from "unburned" to "burned" and is added to the fire front. The fire spread rule is applied for all "burned" cells within the fire front. If a neighboring cell is already in a "burned" state due to another fire front, the model does not propagate fire into that cell. However, this indicates that the two fires have merged into a bigger fire front at that time step. The fire front progressively grows until u is higher than P_s at all neighbors, or if it reaches a cell that has a firebreak condition, where a cell is not allowed to change its state from "unburned" to "burned".

Firebreaks are landscape features that can impede fire spread and decrease the probability of local fire ignition. Rivers and other water bodies are one of the most common natural firebreak agents in landscapes (e.g. Barrett et al., 2013). *WildfireGenerator* is capable of accounting for firebreak rivers by looking at their upstream drainage area, and cells that have a drainage area higher than a defined threshold (A_{fb}) are considered as firebreak agents. Consequently, the model prevents the fire front from crossing cells with a drainage area higher than A_{fb}. To identify firebreak rivers, the *WildfireGenerator* requires a flow accumulator component in Landlab that generates a drainage area field. The model's drainage area default to consider a cell as firebreak river is 2 x 10^5 m^2, but since this value varies for different regions, it can be defined whenever *WildfireGenerator* is initialized.

The *WildfireGenerator* accounts for the natural variability in fire severity for any chosen aridity. For every fire, the model draws a random sample from a normal distribution, using the input aridity as the mean of the distribution and a standard deviation of 0.05. The vegetation field is updated in all cells within the fire front according to the calculated severity (Eq. 5). Since the fire partially (or totally) removes the vegetation, after a single fire, the probability of another fire to ignite or spread through that cell is smaller and increases over time as vegetation recovers.

Vegetation recovery is automatically connected to aridity (Table 1), which defines the rate of post-fire regrowth. After the vegetation is removed by a fire, vegetation recovery takes place and at each time step, a parcel of vegetation is added to the vegetation field. The vegetation field is continuously incremented until it reaches the maximum fuel availability (when $f_a = 1.0$), or if a fire occurs and removes the vegetation again, which will restart the recovery process. The vegetation recovery rates vary as a function of total recovery time t_r and the regrowth exponent r (Eq. 6), controlled by the aridity value in the simulation.

https://doi.org/10.5194/egusphere-2026-3521
Preprint. Discussion started: 3 August 2026

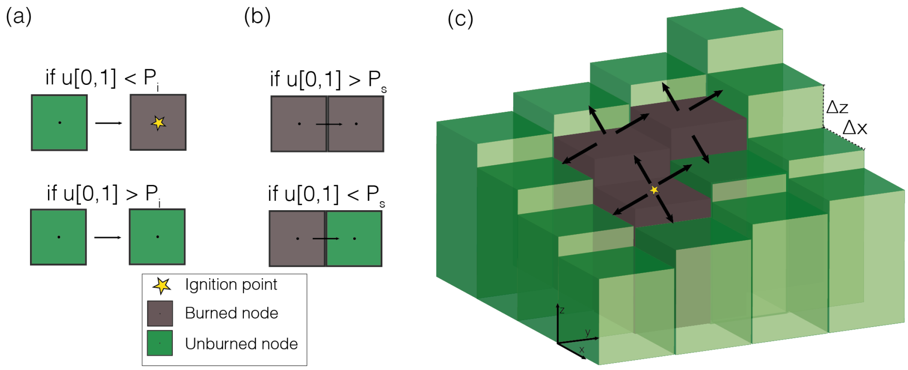

Figure 6. (a) Fire ignition mechanism for a randomly chosen node. A pseudorandom number 'u' between 0 and 1 is generated, and if the number is lower than the probability for ignition (P_i), a fire starts at that node. (b) After the fire ignites at the ignition node, the model generates another pseudonumber 'u' for its neighbours, and the fire spreads if 'u' is smaller than the probability for spread (P_s). (c) Three-dimensional illustration of the fire propagation front. While grey cells with arrows represent burned areas, green cells are not affected by a fire at that timestep.

.

4.2 Landscape evolution modelling framework

Here, we implemented *WildfireGenerator* coupled with components for channel erosion, hillslope diffusion, and soil production from bedrock in FireLands. Channel erosion and hillslope diffusion change according to fuel availability (see Figure 2). FireLands is based on conservation of mass equations that simulate the evolution through time t of topographic elevation z, bedrock surface elevation z_b, and sediment thickness h:

$$\frac{\partial z}{\partial t} = \frac{\partial z_b}{\partial t} + \frac{\partial h}{\partial t} \quad (9)$$

$$\frac{\partial z_b}{\partial t} = U - P \quad (10)$$

$$\frac{\partial h}{\partial t} = \frac{\rho_{bedrock}}{\rho_{soil}} P + D - E \quad (11)$$

where U is the uplift rate of bedrock surface [LT^{-1}], P is soil production rate from bedrock [LT^{-1}], $\rho_{bedrock}$ is bedrock density [ML^{-3}], ρ_{soil} is soil density [ML^{-3}], E and D are the local erosion and deposition rates [LT^{-1}], respectively. E is a combination of E$_f$ for the sediment term of fluvial erosion and E$_h$ for hillslope erosion. For simplicity, we assume that bedrock and soil densities are equal.

https://doi.org/10.5194/egusphere-2026-3521
Preprint. Discussion started: 3 August 2026

4.2.1 Channel erosion

To simulate erosion and deposition by fluvial processes, FireLands uses *SpaceLargeScaleEroder*, an updated version of the Stream Power With Alluvium Conservation and Entrainment (SPACE) component (Shobe et al., 2017). SPACE is a mass conservative stream-power model that simulates sediment erosion and deposition and simultaneously evolves a sediment layer and a bedrock bed in Landlab. Here, we focus on the sediment erosion term of SPACE:

$$E_f = K_{sed} q S^n (1 - e^{-H/H_{*fluv}}) \tag{12}$$

K_{sed} [L^{-1}] is the sediment erodibility coefficient, q is the water discharge per unit width and is calculated as $q = k_q A^m$, where k_q is a coefficient incorporated into K_{sed}, A is the contributing drainage area, and m is the drainage area exponent. S represents the channel slope [LL^{-1}], and n is the slope exponent. H [L] is the thickness of the bed sediment and H_{*fluv} [L] is the bedrock roughness length scale. Here, we use Eq. 7 to dynamically update K_{sed} value in the sediment erosion term of SPACE (Eq. 12). When H is sufficiently low relative to H_{*fluv}, rivers will also erode bedrock. However, in this framework fires do not enhance bedrock incision (see SPACE bedrock erosion term in Shobe et al. (2017)).

At every timestep, K_{sed} is calculated for every core node based on their values of fuel availability f_a (Eq. 7). K_{sed} increases after a fire consumes f_a, and decreases over time while vegetation recovers. In FireLands, K_{sed} is indirectly affected by aridity, as the latter regulates f_a, controlled by the interactions between fires and vegetation regrowth (see Table 1). Note that K_{sed} is constant over time in the fire breaking rivers, as they are not directly affected by vegetation removal.

4.2.2 Non-linear hillslope diffusion

Sediment transport in hillslopes through creep and dry-ravel processes is simulated using a nonlinear depth-dependent transport law. There are several numerical methods available for simulating nonlinear hillslope fluxes (e.g. Perron, 2011; Ganti et al., 2012; Ren et al., 2026). FireLands uses *DepthDependentTaylorDiffuser*, which calculates sediment transport rates following Ganti et al. (2012) with a multi-term Taylor series expansion (for more information about this component, see Barnhart et al. (2019)).:

$$E_h = -DSH^* (1 + \left[\frac{S}{S_c}\right]^2 + \left[\frac{S}{S_c}\right]^4 + ... + \left[\frac{S}{S_c}\right]^{2(n-1)})(1 - e^{-H_s/H^*}) \tag{13}$$

Where D is diffusivity [L^{2}T^{-1}], S is the local slope [LL^{-1}], H^* is the soil transport decay depth, S_c is the critical slope [LL^{-1}], and n is the user-defined number of terms used in the approximation. Similarly to the effects of fires on erosion by fluvial processes, D varies according to the value of fuel availability f_a (Eq. 8), which increases after a fire and decays as vegetation recovers. The duration of post-fire increase in D depends on aridity, since it controls the rate of vegetation recovery (Table 1).

https://doi.org/10.5194/egusphere-2026-3521
Preprint. Discussion started: 3 August 2026

Table 2. List of parameters used for the main simulations evaluating only *WildfireGenerator* component.

Parameter	Description	Value
Rows (-)	Number of grid rows	200
Columns (-)	Number of grid columns	240
Δx (m)	Cell spacing	50
Δt (yr)	Time step	1
t_{run} (yr)	Total run time	Varying per simulation
a (-)	Aridity	Varying per simulation
Pot_i (-)	Number of potential fires per time step	80
A_{fb} (m^2)	Drainage area threshold for firebreak rivers	2 x 10^5

4.2.3 Soil production

Conversion of bedrock into soil is represented using an exponential function of the soil thickness (Heimsath et al., 1997; Dixon et al., 2009). To represent soil production P, FireLands uses *ExponentialWeatherer* component in landlab:

$$P = P_0 \exp(-\frac{h}{h_p^*}) \tag{14}$$

Where P_0 is the maximum soil production rate, h is soil thickness, and h_p^* is a characteristic weathering depth. *WildfireGenerator* does not directly change soil production efficiency in Eq. 14, however, it does influence soil production efficiency, as soil thickness is modified throughout the landscape due to post-fire erosion and deposition.

5 Verification and evaluation

FireLands simulates co-evolving landscapes and vegetation patterns through a combination of our new *WildfireGenerator* component and parameter modifications of existing Landlab components simulating uplift, erosion, transport of sediment and soil production from bedrock. We test and showcase the performance of FireLands in two stages. First, we describe the behavior of wildfires and their impact on vegetation patterns as such, without considering their impact on erosion and sediment transport. Second, we run the FireLands landscape evolution model in full to showcase how the model captures the coupling between fires and sediment dynamics in evolving landscapes.

https://doi.org/10.5194/egusphere-2026-3521
Preprint. Discussion started: 3 August 2026

5.1 Evaluation of the fire component

5.1.1 Synthetic wildfires

We start by applying *WildfireGenerator* to synthetic landscapes. Here, our goal is to evaluate whether the cellular automata model component is capable of reconstructing vegetation patterns consistent with field observations under various aridities and whether feedbacks between aridity and fire frequency follow theoretical predictions.

For this experiment, we create a steady state landscape using a Landlab raster model grid of 200 by 240 nodes, with a spatial resolution of 50 m. The model is run with open boundary nodes along the top and bottom edges, closed boundaries at the left and right edges, detachment-limited incision (FastScapeEroder) and nonlinear diffusion (TaylorNonLinearDiffuser). The maximum relief in steady state is 1525 m, and due to the boundary conditions, all catchments have a north-south orientation. Here, fire behavior is not influenced by catchment orientation, as aspect does not play a role in fire activity in the current version of *WildfireGenerator*. Once the model reaches topographic steady state, a fuel availability field is added. A summary of all parameter values used in this experiment is provided in table 2.

First we evaluate how fuel availability evolves over time under different aridity conditions. Different aridity values scale with severity (Eq. 4), are linked to fire frequency (Fig. 1) and control vegetation recovery (Table 1). Here, three aridity scenarios are defined, and we divide the test into two stages. First, we test the effects of aridity on mean fuel availability ($\overline{f_a}$) over 500 years (Figure 7). Second, we focus on the spatial distribution of fuel availability under each aridity scenario over the first 100 years of simulation (Figure 8). We use low aridity ($a = 0.09$) to mimic low severity, low fire frequency and fast vegetation recovery, intermediate aridity ($a = 0.5$) to represent high fire frequency and moderate severity, and high aridity ($a = 1.0$) to mimic high severity and slow vegetation recovery. For all aridity scenarios, we start the model with the fuel availability field using the same reproducible random seed value ($\overline{f_a} \approx 0.4$) on top of the steady state topography. We run *WildfireGenerator* for 500 years to evaluate the evolution of fuel availability over this period. All other component parameters remained the same (see table 2).

For all aridity scenarios, there is an initial increase in fuel availability (Figure 7). As the system evolves, individual pixels become increasingly connected through periods of uninterrupted growth. Following this transient phase of fuel accumulation, vegetation patterns start to enable the emergence of larger and more connected fuel loads that support extensive fire events. Consequently, mean fuel availability stabilizes around a dynamic equilibrium. The period of this transient stage, in which vegetation is still self-organizing from the initial random vegetation pattern is mainly controlled by vegetation growth rates. Vegetation growth is fast under low aridity and progressively slower as aridity increases, resulting in longer periods of vegetation self-organization under high aridity compared to the low and intermediate scenarios. After reaching dynamic equilibrium, periods of increased fire severity are responsible for lowering the mean fuel availability. These periods are more pronounced under high aridity, as fires are typically more severe and vegetation takes longer to reaccumulate. In turn, as aridity decreases, vegetation recovers faster and periods of increased fire activity are less marked over time.

Mean fuel availability ($\overline{f_a}$) at equilibrium decreases with increasing aridity, showing a significant control of aridity on vegetation accumulation (Figure 7). Note that vegetation type changes with aridity (see Table 1): Under low aridity, the vegetation type is "Trees and shrubs" and the combination of fast vegetation recovery, low fire frequency, and relatively small fires sets

https://doi.org/10.5194/egusphere-2026-3521
Preprint. Discussion started: 3 August 2026

$\overline{f_a}$ to stabilise close to the maximum value (≈ 1) (Figure 7). At intermediate aridity, vegetation shifts from "Trees and shrubs" to "Dense shrubs" (Table 1). The vegetation regrowth rates are still fast enough to recover a significant part of the vegetation before the next fire occurs. $\overline{f_a}$ stabilises at ≈ 0.7 in the intermediate aridity scenario (Figure 7). This is mainly driven by the increase in fire severity from low to intermediate aridity, where on average each fire removes a larger amount of vegetation and therefore lowering $\overline{f_a}$. For the high aridity scenario, vegetation type changes from "Dense shrubs" to "Sparse shrubs" (Table 1). Post-fire vegetation recovery rates at high aridity are the lowest of all aridity scenarios and vegetation becomes a limitation for fire frequency. Despite the decrease in fire activity under high aridity, $\overline{f_a}$ stabilises at ≈ 0.5 (Figure 7), resulted from the combination of high fire severity and low vegetation recovery rates. In this way, under high aridity, the slow vegetation recovery between fires limits $\overline{f_a}$ to $\approx 50\%$ of its maximum capacity (Figure 7).

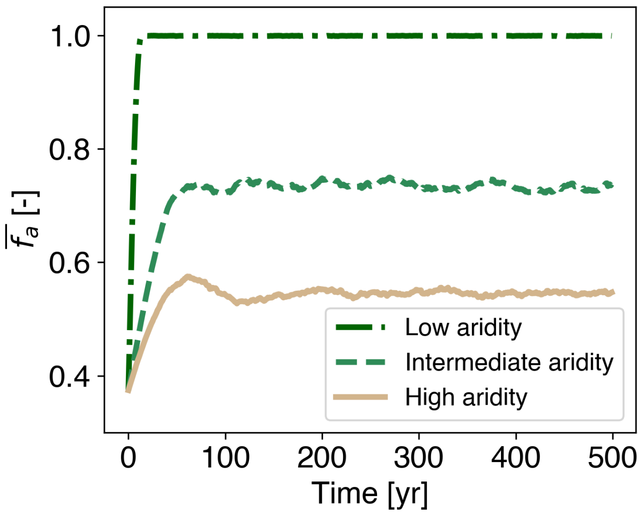

Figure 7. Comparison of mean fuel availability under different aridity conditions. At low aridity, fuel availability is near its maximum potential due to faster vegetation recovery and a low frequency of moderate- to high-severity fires. fuel availability decreases at intermediate aridity due to a combination of increased fire activity and severity. At high aridity, vegetation takes longer to reach a dynamic steady-state condition due to the high frequency of high severity fires and lower rates of recovery.

.

Spatial patterns of vegetation evolve differently under various aridity scenarios. Figure 8 shows the spatial evolution of vegetation during the first 100 model years under the three previously defined aridity scenarios. Under low aridity, high density vegetation is not available to burn due to the high moisture content (Figure 8a-c). Due to favorable growing conditions, $\overline{f_a}$ quickly increases towards 0.99 at 40 years under low aridity conditions (Figure 8b). $\overline{f_a}$ stabilizes at 0.99 until 100 years, with few visible low severity burned patches in the landscape (lighter green areas in Figure 8b-c). This suggests that at 40 years vegetation has already reached dynamic equilibrium with (limited) fire activity (Figures 7 and 8b).

https://doi.org/10.5194/egusphere-2026-3521
Preprint. Discussion started: 3 August 2026

Under intermediate aridity, moisture decreases and vegetation becomes more combustible. There is an increase in burned area and soil exposure, indicated in Figure 8 by decreased fuel availability, under intermediate aridity (grey areas in Figure 8d-f) due to the combined increase in fire frequency and severity in this scenario. A clear difference in vegetation patterns emerges between low and intermediate aridity at 40 years. Vegetation is less dense under intermediate aridity ($\overline{f_a}$ = 0.68), showing more visible signs of fire activity, as areas with a higher percentage of bare soil start to appear in the landscape. However, at 40 years vegetation is not yet in equilibrium with fires under intermediate aridity, reaching this state between 40 and 100 years, confirmed by the $\overline{f_a}$ plateau in Figure 7. After 100 years under intermediate aridity, vegetation has reached dynamic equilibrium with the highest fire activity of all scenarios (see the peak in the fire frequency curve when $a \approx 0.5$ in Figure 9). At 100 years, fire has affected almost the entire landscape, but vegetation recovery is still fast enough to prevent vegetation from being scarce. Overall, intermediate aridity shows a fire-vegetation recovery feedback where vegetation is able to reach equilibrium with increased fire activity while maintaining its connectivity throughout the landscape.

Under high aridity conditions, fire severity increases, and vegetation recovery rates are the lowest of all aridity scenarios. At 40 years under high aridity, vegetation is still evolving to equilibrium with fires. Dynamic equilibrium is reached at 100 years (see Figure 7) with $\overline{f_a} = 0.54$, and the combination of high fire severity and low vegetation recovery rates translates into sparse vegetation, with the highest percentage of exposed (or bare) soil appearing in the landscape (Figure 8i). Although vegetation exhibits the highest susceptibility to burning under high aridity, there is a decline in fire frequency beyond an aridity of ca. 0.5 (Figure 9b). We attribute this behavior to vegetation limitation in high aridity landscapes (Figure 8g-i), with the lower $\overline{f_a}$ of all aridity scenarios. In these conditions, each fire removes a substantial fraction of the already sparse vegetation while low post-fire recovery rates prevent biomass from re-accumulating across the landscape. As a result, vegetation availability driven by aridity, rather than aridity-driven fire activity, becomes the primary constraint for fire activity under the high aridity scenario.

As a second test, we evaluate the impact of aridity on fire frequency. This is tested by running 20 fire simulations over 500 years using 20 different constant aridity values evenly spaced between 0 and 1, while the other parameters are constant (see table 2). The simulated fire frequency for each aridity value is shown in Figure 9b. A clear increase in fire frequency is shown when aridity increases from a value of 0 to 0.5 where a rollover occurs, followed by a clear decrease in fire frequency. Although vegetation is abundant when $a \approx 0$, high moisture results in low fire frequency. When $a \approx 0.5$, vegetation remains at a high density, however, lower moisture makes vegetation available to burn, causing a peak in fire frequency. As aridity increases to $a \approx 1$, fuel availability decreases and becomes a limitation for fire ignition, resulting in a decay in fire frequency, as shown in Figure 9. However, the fire frequency is still slightly higher than predicted by the theoretical predictions (dotted line in Figure 9). This slight offset can be explained by different levels of vegetation availability between the current version of *WildfireGenerator* and the conceptual model of Pausas and Ribeiro (2013). In *WildfireGenerator*, vegetation is still able to regrow when $a = 1$, which may not be the case for very arid regions in real landscapes. Overall, our aridity test matches the conceptual fire-aridity described by Pausas and Paula (2012) well despite slightly higher simulated frequencies at high aridity (Figure 9). These results demonstrate that our simplified cellular automata model effectively replicates fire frequency across an aridity gradient.

https://doi.org/10.5194/egusphere-2026-3521
Preprint. Discussion started: 3 August 2026

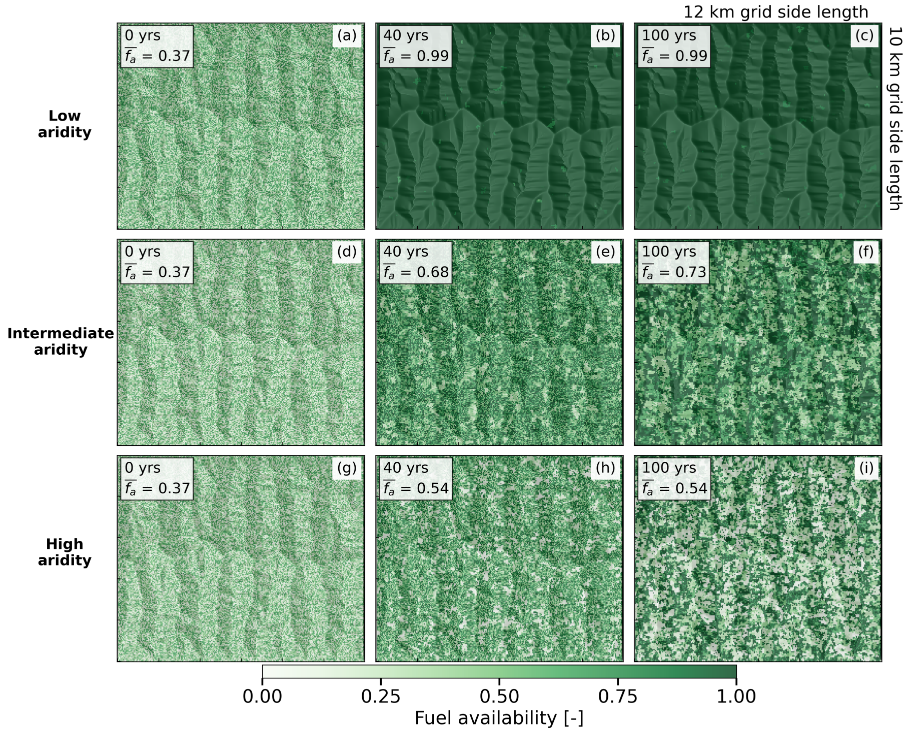

Figure 8. Snapshots of fuel spatial distribution in a synthetic topography at three times (0, 40 and 100 years) under three aridity scenarios. FireEroder was instantiated to simulate fuel evolution starting from the same random reproducible seed. Fuel is denser and less affected by fires at low aridity. At intermediate aridity, vegetation remains well connected, but patches of bare soil (grey areas) appear. At high aridity, fuel is sparsely distributed with an expansion of bare soil throughout the topography.

.

5.1.2 Fit to real wildfire data

To test the performance of our model in real landscapes, we compare a measured frequency-magnitude fire distribution with a modelled one using WildfireGenerator (Figure 10). We use an inventory of mapped fires in southern Calabria, a Mediterranean landscape in southern Italy that is frequently affected by fires. The inventory is provided by the European Forest Fire Information System (EFFIS, San-Miguel-Ayanz et al. (2012)), which comprises 683 mapped fires over a 16-year period (2008-2024) with sizes ranging from 1 to 7000 hectares. To generate the synthetic data, we use *WildfireGenerator* on a 10 meter resolution digital elevation model (DEM) of Calabria (Tarquini et al., 2007).

Additionally, we assessed the influence of topographic relief on simulated fire activity. We derived five topographic scenarios by rescaling the existing DEM of Calabria. These included the original DEM, a flat scenario in which all elevation was removed (0 m) while preserving the spatial extent of the domain, and three intermediate scenarios generated by scaling the original DEM by factors of 0.25, 0.5, and 0.75. All simulations were conducted on grids with identical spatial dimensions and pixel resolution.

https://doi.org/10.5194/egusphere-2026-3521
Preprint. Discussion started: 3 August 2026

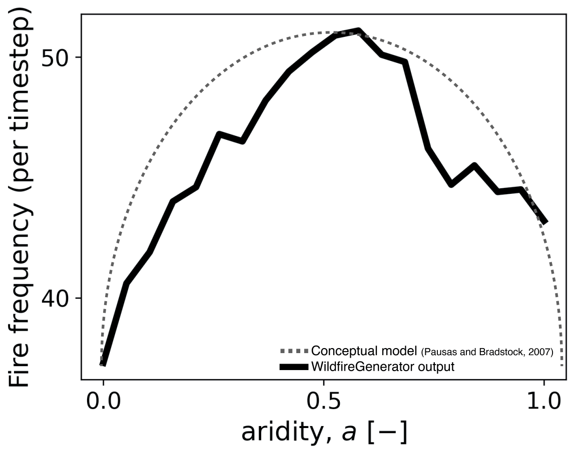

Figure 9. Fire frequency output after running *WildfireGenerator* to simulate fire activity for 20 aridity values, evenly spaced between 0 and 1. In low aridity, vegetation is abundant, but high moisture results in low fire frequency. In intermediate aridity, lower moisture makes vegetation available to burn, causing a peak in fire frequency. In high aridity, fuel availability decreases and becomes a limitation for fire ignition, resulting in a decay in fire frequency

.

For each of the five topographic scenarios tested, we first simulated fuel availability at dynamic equilibrium using *Wildfire-Generator* with default parameter values listed in table 2. After the vegetation reached equilibrium, we run *WildfireGenerator* again for 16 years, the same period comprised by the EFFIS inventory, and plotted the magnitude-frequency distributions for all scenarios. Overall, there is a good correspondence between the modelled and observed fires (Figure 10). The *WildfireGenerator* generates a realistic estimate of small fires, shown by the similar frequency of fires burning between 10^{-3} and 10^{-4}% of the total area. While there is a small overestimation of medium-sized fires that cover between 2x10^{-3} and 2x10^{-4}% of the total area, the *WildfireGenerator* again shows a good representation of larger fires, which affect 5x10^{-1} and 7x10^{-1}% of the grid. However, the largest mapped fires documented in the EFFIS inventory are not reproduced by our model results. Such high-magnitude events typically arise from a confluence of processes, including anthropogenic land-use changes, human-ignitions and wind-driven fire spread. These mechanisms are not represented in the current version of the *WildfireGenerator*, potentially explaining its inability to capture the upper tail of the observed fire-size distribution. We do not observe significant topographic control on the modelled fire frequency-magnitude distributions (Figure 10).

5.2 FireLands: coupling *WildfireGenerator* in a LEM framework

Integrating dynamic fire-behavior models with erosion and sediment transport components in a Landscape Evolution Modelling (LEM) framework provides a powerful tool for quantifying fire-sediment feedbacks across a range of spatial and temporal scales. In the following, we highlight essential characteristics of the FireLands coupled fire-erosion model by simulating

https://doi.org/10.5194/egusphere-2026-3521
Preprint. Discussion started: 3 August 2026

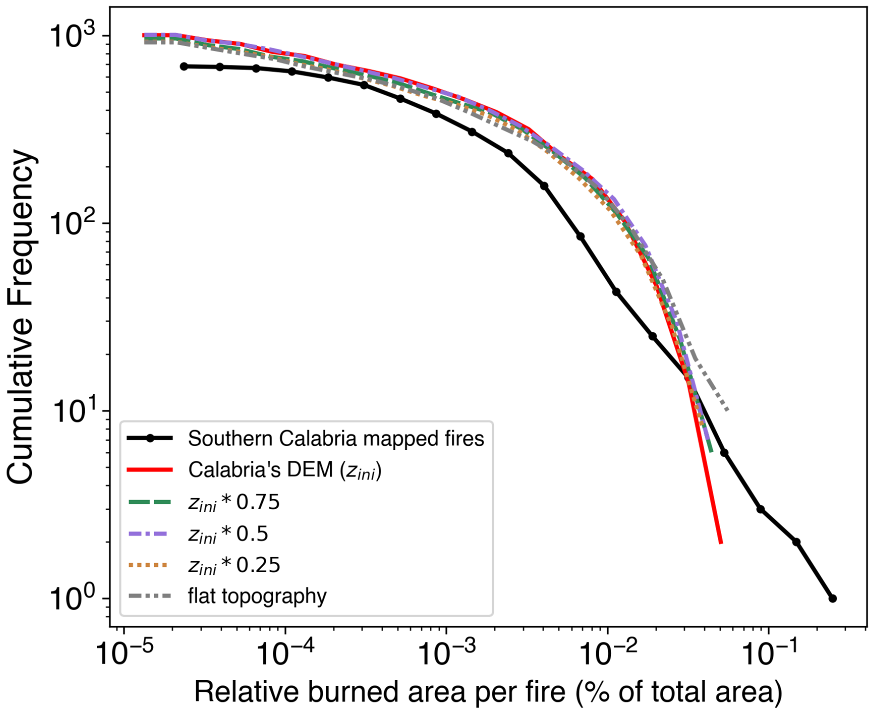

Figure 10. Frequency–magnitude distributions of modelled fires after a 16-year simulation using different topographic settings, compared to a fire inventory from southern Calabria (Mediterranean biome) that comprises the same time interval (EFFIS). We used a 10-meter DEM covering the same area as the fire inventory, and used the same parameters for five different relief scenarios (flat topography, and relief scaled by 0.25, 0.5 and 0.75)

.

the impact of fires on synthetically evolving topography. To do so, we run the FireLands LEM starting from the same synthetic steady state topography as the one used in previous tests (see section 4.1.1). We evolve the fuel availability to dynamic equilibrium using *WildfireGenerator* considering fire regimes corresponding to low, intermediate, and high aridity. For FireLands initial conditions, we add a 1 meter thick sediment layer homogeneously distributed in the landscape (0 yr snapshots in Figure 11). FireLands simulates landscape evolution through channel incision and deposition (SpaceLargeScaleEroder) and non linear hillslope diffusion (DepthDependentTaylorDiffuser). Total model run time is 100 years with a time step of 1 year. All the parameter values are listed in Table 3. During the simulation of each aridity scenario, we kept track of changes in sediment thickness (Figure 11), changes in topographic elevation (Figure 12) between the initial (0 years) and current topography at 40 and 100 years, sediment redistribution along a valley cross-section (Figure 14) and catchment-average sediment yield for the biggest catchment in the grid (Figure 15).

https://doi.org/10.5194/egusphere-2026-3521
Preprint. Discussion started: 3 August 2026

Table 3. List of parameters used for the main simulations in FireLands landscape evolution model.

Parameter	Description	Value
Rows (-)	Number of grid rows	200
Columns (-)	Number of grid columns	240
Δx (m)	Cell spacing	50
Δt (yr)	Time step	1
t_{run} (yr)	Total run time	Varying per simulation
H_{ini} (m)	Initial soil thickness	1
U (m yr^{-1})	Uplift rate	1 x 10^{-3}
K_r (m^{-1})	Bedrock erodibility	1 x 10^{-5}
K_{sed_0} (m^{-1})	Sediment erodibility base level	1.5 x 10^{-5}
K_{boost} (-)	Post-fire sediment erodibility maximum fold increase	100
m (-)	Slope exponent	0.45
n (-)	Area exponent	1
H_{*fluv} (m)	Bedrock roughness length scale	1
ϕ_{sed} (-)	Sediment porosity	0
F_f (-)	Fraction of fine fluvial sediment	0
V_s (m yr^{-1})	Effective settling velocity	1 x 10^{-3}
P_0 (m yr^{-1})	Maximum soil production rate	1 x 10^{-3}
H_* (m)	Soil production decay depth	0.44
D (m^2 yr^{-1})	Diffusivity	0.1
D_{boost} (-)	Post-fire diffusivity maximum fold increase	10
S_c (m/m)	Critical slope threshold	1.0
a (-)	Aridity	Varying per simulation
Pot_i (-)	Number of potential fires per time step	80
A_{fb} (m^2)	Drainage area threshold for firebreak rivers	2 x 10^5

https://doi.org/10.5194/egusphere-2026-3521
Preprint. Discussion started: 3 August 2026

5.2.1 Sediment thickness redistribution

Sediment thickness redistribution clearly documents the impact of wildfire driven erosion (Figure 11). There is a tendency for sediment to be transported from hillslopes to river channels. Most of the deposition occurs at rivers that have a drainage area above A_{fb}, the threshold for firebreak rivers. Because fires terminate at firebreak rivers, erosion parameters remain unaffected at these locations, leading to an excess of incoming sediment and localized deposition. The amount of deposition in these rivers depends on how much sediment is mobilized after a fire occurs within their contributing areas.

The low aridity scenario shows the lowest changes in sediment redistribution throughout the landscape (Figure 11a-c). We observe that even with little fire activity, it is possible to see an increase in sediment thickness in the main rivers, considered the firebreak rivers, and a slight decrease in hillslope sediment cover at 40 years. This behavior persists after 100 years, with a modest additional increase in river sediment thickness, as hillslopes still experience a decrease in sediment cover. In low aridity, $\overline{h}$ changes from 1 to 0.89 m, a 11% decrease in 100 years.

Under intermediate aridity, fires become more erosive, fire severity increases (Eq. 4) and mean fuel availability decreases (Figures 11d-f). This implies larger sediment redistribution and highly heterogeneous and overall lower sediment thickness after 40 years compared to the low aridity scenario (Figure 11e). At 100 years, $\overline{h}$ decreases 36%, and sediment deposition in the main rivers becomes more prominent (Figure 11e).

Under high aridity, we find the largest increase in sediment transport (Figure 11g-i). After 40 model years (Figure 11h), 29% of the initial sediment thickness is eroded at various locations and the spatial distribution of sediment thickness throughout the grid is highly heterogeneous (Figure 11i). At 100 years, there is an average decrease of 55% in sediment thickness due to fire activity, and most of the sediment on the hillslopes is evacuated from the catchments or deposited in the main rivers (Figure 11i).

5.2.2 Changing topography

Wildfires drive topographic change with aridity exerting a primary control on erosion and deposition (Figure 12). Under low aridity conditions, almost no elevation difference is shown after 40 years (Figure 12b), and most of the topographic change is between 0 and 0.1 m. There is a slight increase in elevation differences after 100 years, with erosion perceptible mainly near the hilltops (red cells in Figure 12c). This reflects the combination of little fire activity and typically low severity fires under low aridity.

After 40 years under intermediate aridity (Figure 12e), fire-related erosion produced bigger changes in elevation. At 40 years, all catchments are already affected by post-fire erosion and the main river channels show signs of sediment deposition (blue cells in Figure 12e). After 100 years, the fire activity resulted in deposition of up to 0.3 m along the main rivers (Figure 12f), also higher compared to the low aridity scenario. Hillslope erosion was also enhanced, reaching a negative 0.5 m elevation difference between the initial and final topography.

High aridity conditions produced the biggest changes in elevation after 40 years (Figure 12h). Although the fire frequency is lower than the intermediate aridity, the increased fire severity and low vegetation recovery rates result in persistent fire-

https://doi.org/10.5194/egusphere-2026-3521
Preprint. Discussion started: 3 August 2026

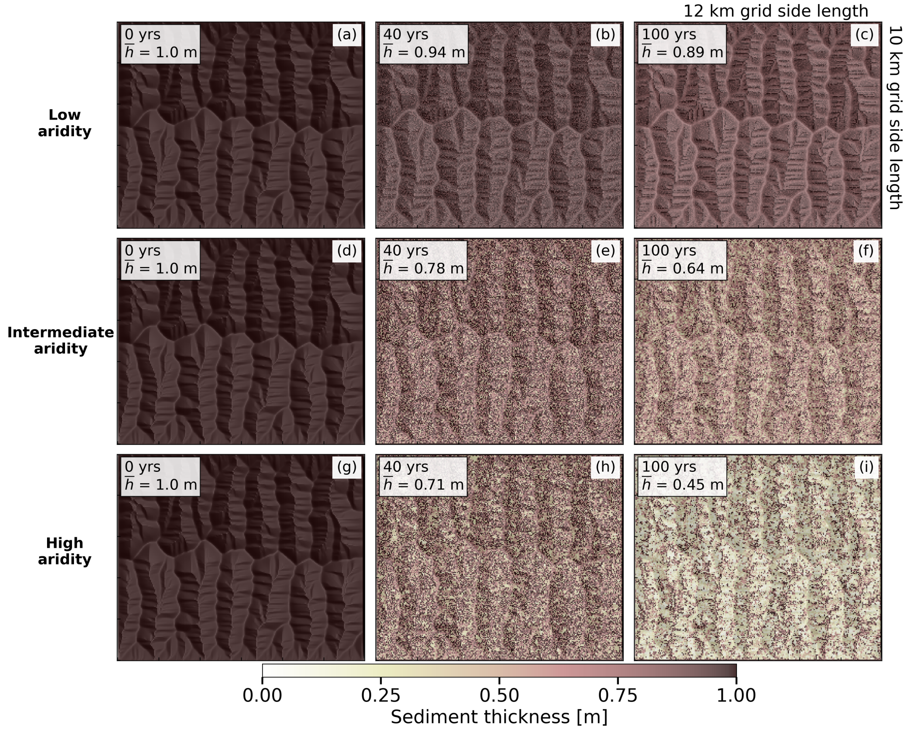

Figure 11. Snapshots of sediment thickness spatial distribution at 0, 40 and 100 years for each aridity scenario. There is an overall tendency for sediment to be transported from hillslopes and accumulate at river channels. This behaviour intensifies as aridity increases, with the high aridity scenario showing the thinnest sediment layer at hillslopes, and the thickest layer at the main channels.

related sediment transport throughout the landscape. At 100 years, a large proportion of the hillslopes lost ≈ 1.0 m elevation (Figure 12i), which is the initial sediment thickness added to the topography (see Figure 11). This shows that under high aridity, there is a tendency towards low sediment availability in the hillslopes as soils undergo rapid thinning, which could limit further erosion on longer timescales. In this scenario, soil production gains importance, as it controls whether, under this erosion dynamics, the landscape remains soil-mantled or transitions to a bedrock landscape.

5.2.3 Sediment transport and fire-vegetation feedbacks

Erosional dynamics in the landscape are controlled by fire-vegetation feedbacks, primarily regulated through aridity. To get a clear picture of how aridity controls fires, vegetation and sediment transport, we zoomed in on the biggest catchment off the grid after 100 model years (Figure 13). There is a clear connection between vegetation patterns and sediment transport dynamics, where sediment transport increases as fuel availability decreases (Figures 13a, d, g). As fuel availability decreases in the landscape, sediment transport through overland flow and gravity-driven hillslope processes becomes more pronounced. These post-fire geomorphic processes are reflected in the topography as overland flow feeds the main rivers with sediment

https://doi.org/10.5194/egusphere-2026-3521
Preprint. Discussion started: 3 August 2026

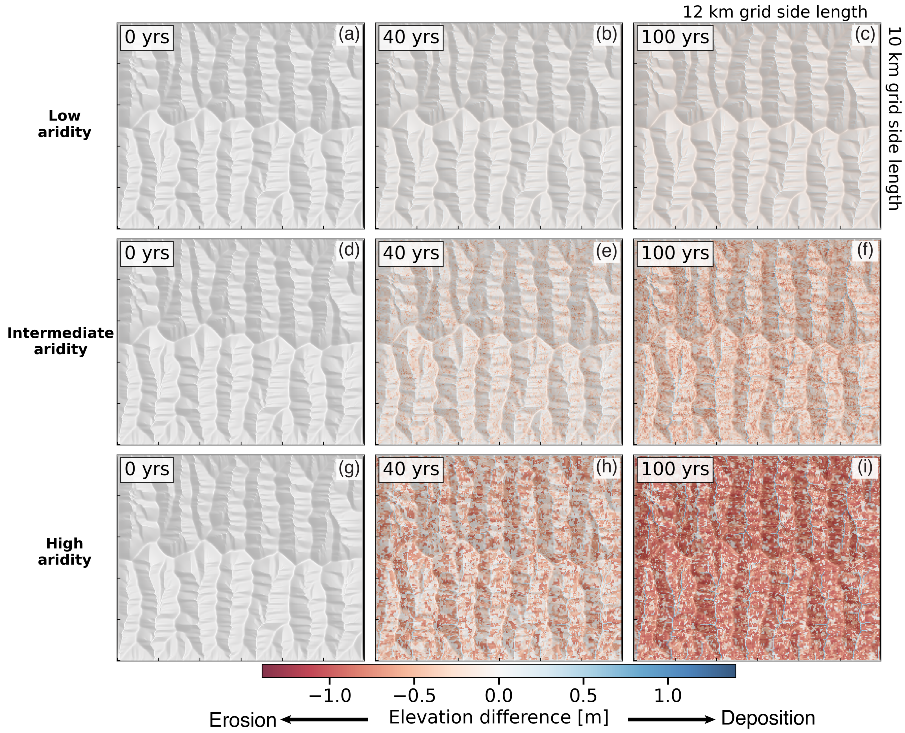

Figure 12. Snapshots of elevation differences between the initial topography (at 0 years), and the topography at 40 and 100 years for each aridity scenario. The fire activity drives erosion at the hillslopes (negative elevation difference), with the sediment being deposited in the rivers. Sediment transport from hillslopes to rivers is mainly driven by high erodibility and diffusivity values, which rise with increasing aridity.

detached from the hillslopes, and the sediment mobilized by non linear diffusion on hillslopes is deposited along the same river valleys (Figure 13b, e, h). The sediment transport dynamics influence sediment thickness spatial distribution, as the material is removed from the hillslopes and accumulates in the rivers (Figure 13c, f, i).

In real landscapes, post-fire erosion could reach five orders of magnitude higher than pre-burn state (Orem and Pelletier, 2016; Santi and Rengers, 2020; McGuire et al., 2024). The average erosion rates in the model grid before fire activity is 0.5 mm yr^{-1}. After 100 years, there is an up to an order of magnitude increase in average erosion rates (6 mm yr^{-1} in high aridity) (Figure 13b, e, h), and . This increase is comparable to post-fire changes in erosion in landscapes such as western (Abrahams et al., 2018; Rengers et al., 2021) and continental United States (Orem and Pelletier, 2016).

As previously discussed (see also Figure 11), there is a tendency for soil thinning on hillslopes and sediment accumulation at the river valley across aridity scenarios. Even in the low aridity scenario, the smallest fire activity is capable of triggering sediment transport from hillslopes to rivers (Figure 14). Under low aridity, the sediment layer is still ≈ 1.0 m across the valley, with a slight increase in the river. As aridity increases to intermediate and high levels, the soil layer on the hillslopes becomes

https://doi.org/10.5194/egusphere-2026-3521
Preprint. Discussion started: 3 August 2026

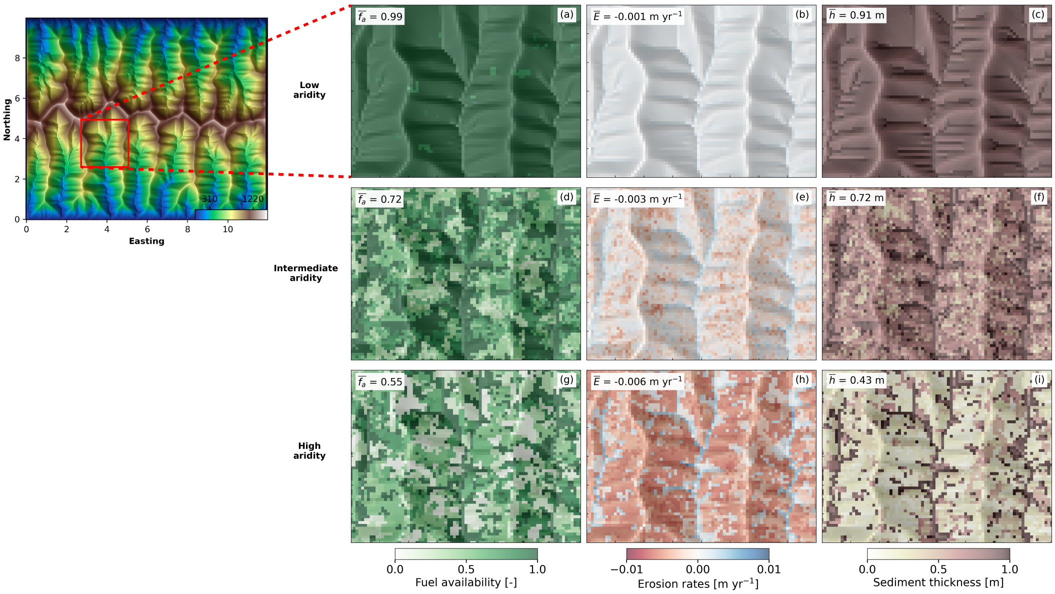

Figure 13. Snapshots of fuel availability, erosion rates and sediment thickness at 100 years, zoomed at a selected portion of the model domain. As aridity increases, fuel availability is lower and has low connectivity. Sediment transport from hillslopes to rivers increases, which is translated to sediment loss in the hillslopes and aggradation in the rivers.

thinner due to the increase in post-fire erosion. Under high aridity, with a persistent increase in erodibility and diffusivity due to the high incidence of high-severity fires and low vegetation recovery rates, soil thickness decreases to virtually zero at several points across the valley. Despite high erosion rates, a very thin soil layer remains in place. As soil thickness decreases to virtually zero, soil production rates increase exponentially, explaining the sustained soil layer even in a scenario of rapid transport.

5.2.4 Catchment wide sediment fluxes

Changing aridity, and therefore fire regimes, affects not only sediment redistribution within the catchment, but also sediment yield exported from the biggest catchment outlet (Figure 15). At 0 years, steady state sediment yield at the biggest catchment outlet is ≈ 0.1 x $10^5 \mathrm{m}^3 \mathrm{yr}^{-1}$. After adding the initial imposed sediment thickness (of 1 meter depth), the catchment-average sediment yield evolved differently according to each aridity scenario. Under low aridity, experiencing little fire activity and low severity fires, sediment yield shows minimal changes relative to pre-fire steady state conditions. Under intermediate aridity, sediment yield increases to 0.3 x $10^5 \mathrm{m}^3 \mathrm{yr}^{-1}$, three times higher than steady state values. After the rapid increase, sediment yield dynamically equilibrates at ≈ 0.3 x $10^5 \mathrm{m}^3 \mathrm{yr}^{-1}$.

Under high aridity, sediment yield quickly reaches a peak of ≈ 0.9 x $10^5 \mathrm{m}^3 \mathrm{yr}^{-1}$, a nine-fold increase in steady state fluxes. Instead of stabilizing in this new value, the rapid increase is followed by a general decrease in sediment yield. As fire regimes remain constant within each aridity scenario, the decreasing trend is attributed to sediment-availability constraints.

https://doi.org/10.5194/egusphere-2026-3521
Preprint. Discussion started: 3 August 2026

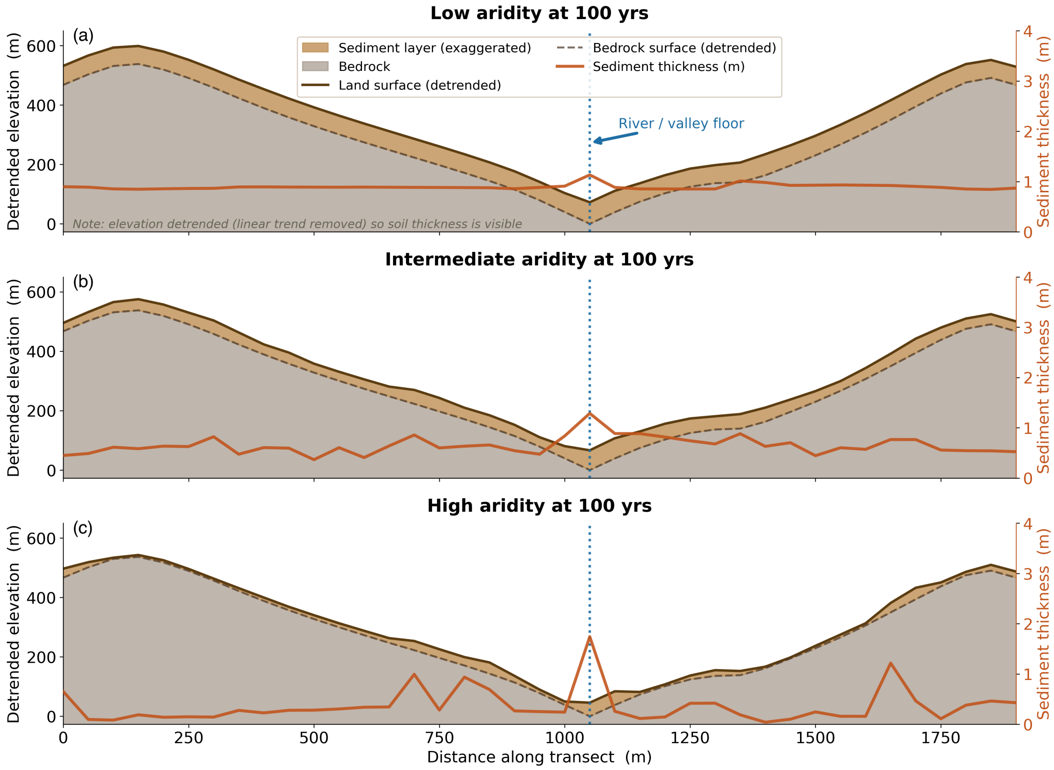

Figure 14. Sediment thickness after 100 years under each aridity scenario at a valley within the biggest catchment in the grid. Sediment redistribution shows deposition at the river/valley floor (blue dotted line), and erosion at the hillslopes. The magnitude of hillslope erosion and river deposition increases with aridity.

In particular, soil production rates are insufficient to replenish sediment removed by successive fires, thereby progressively limiting sediment transport. Within the decreasing trend, additional small peaks in sediment yield occur over time. These are caused both by the occurrence of fires in areas that were not previously burned and by the erosional response to high magnitude, high severity fires. High aridity areas usually present slower erosion rates compared to intermediate aridity due to limited sediment availability (Noske et al., 2024). Our model results show that, from a scenario where sediment availability does not initially constrain sediment fluxes, high aridity fire regimes have a bigger erosional power, mainly due to increased fire severity (Benavides-Solorio and MacDonald, 2005). As soon as low sediment availability limits erosion, sediment fluxes start to decrease substantially (Fig. 15).

6 Limitations

Currently, the FireLands wildfire component does not account for seasonal changes in fire activity (e.g. high fire activity during dry summers and vegetation replenishment during wet winter). Instead, FireLands works on a yearly timescale, which

https://doi.org/10.5194/egusphere-2026-3521
Preprint. Discussion started: 3 August 2026

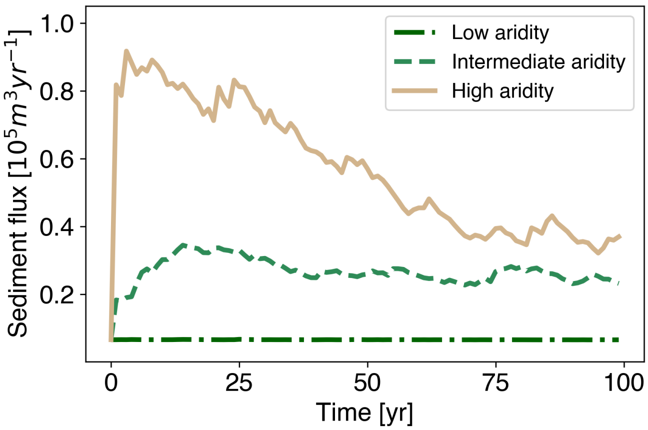

Figure 15. Mean sediment fluxes from the biggest catchment in the grid over a 100-year simulation, changing only aridity values in FireLands. High, intermediate and low aridity scenarios were tested using the same initial model parameters and soil depth distribution. While low aridity produces the lowest erosion rates of all scenarios, the biggest increase in fluxes at high aridity is driven mostly by the increased number of high severity fires in this scenario.

makes the model suitable for simulating the fire-vegetation-erosion feedbacks over time scales ranging between 10^1-10^6 years. Although the aridity and fuel availability weighting represent well theoretical predictions of fire activity along an aridity/productivity gradient, the explicit incorporation of a productivity term into *WildfireGenerator* would also be helpful to improve the model performance in high aridity environments (e.g. Nudurupati et al., 2023). Additionally, the *WildfireGenerator* does not simulate specific fire spread conditions such as wind, which can be incorporated in future versions (see Rothermel, 1972; Freire and DaCamara, 2018). Including the effect of these weather conditions could improve the capability of *WildfireGenerator* generate larger fires, as fuel availability and/or large river are not firebreaks under extreme fire weather/behavior. The impact of human activity on suppressing and/or igniting fires is also not accounted for in the current version of the model.

Regarding post-fire geomorphic processes, FireLands does not simulate post-fire landslides and debris flows. However, as it is built within Landlab framework, FireLands is capable of incorporating any newly developed component that simulates post-fire geomorphic processes. Currently, FireLands uses traditional geomorphic transport models formulated for long-term landscape evolution, which are appropriate to describe sediment fluxes at annual to decadal scales (Ariagno et al., 2025). Yet, a future version of FireLands could benefit from incorporating models that simulate post-fire overland flow and mass wasting in response to rainstorm events (Shmilovitz et al., 2025; Campforts et al., 2022). Additionally, FireLands uses the exponential soil production function (Heimsath et al., 1997), where soil production increases exponentially with decreasing soil thickness. However, there is a current debate on the contribution of different landscape characteristics to soil production, and on whether soil production scales with soil erosion (Geyman et al., 2025). In that case, FireLands could use different soil production relationships. One example is the "humped" function (Anderson, 2002), which soil production peaks at a certain thickness, and decreases again as soil thickness approaches zero. Another alternative is a process-based soil production model based on uplift and rock strength (Geyman et al., 2025). Finally, FireLands simulates how vegetation recovery is controlled by aridity, but this version does not account for how soil thickness regulates vegetation processes (as thin soils could limit post-fire vegetation recovery), or how vegetation can enhance chemical weathering and hence facilitate soil production, which could be simulated using the "humped" relationship between soil thickness and soil production.

7 Potential calibration of FireLands

FireLands is designed to be parameterized for a range of landscapes with different fire-vegetation-erosion feedbacks. Therefore, to make the model applicable in various landscapes, we identify the main categories of potential calibration data. The first category is the vegetation dynamics parameterization, often derived from remote sensing data over multiple spatial and temporal scales. These include landscape heterogeneity in fuels, which can be derived from remote sensing, and post-fire vegetation recovery rates under various aridity/productivity conditions. Moreover, if applied to experiments on regional scales, regional magnitude-frequency distributions of fires are useful for constraining FireLands wildfire parameters. The second category is the calibration of the FireLands erosion term, as additional data quantifying diffusivity and erodibility alterations following a fire. Recent assessments on regional (Vieira et al., 2023) and global (Vieira et al., 2026) post-fire erosion are useful for calibrating FireLands on larger spatial scales. While a wide range of the magnitude of post-fire erosion increase is already documented (McGuire et al., 2024), there is a need of quantifying the erosional enhancement in different aridity conditions (e.g. Noske et al., 2016, 2024). FireLands erosion terms could also benefit from further estimations of the contribution of fires to long-term sediment fluxes (e.g. Roering and Gerber, 2005; Orem and Pelletier, 2016; Rengers et al., 2021).

8 Conclusions

We present FireLands, a new Landscape Evolution Model built by combining a newly developed landlab fire component (*WildfireGenerator*) with already available erosion and deposition components, and models of sediment transport, channel erosion and hillslope non-linear diffusion. *WildfireGenerator* in FireLands is capable of simulating fires of several sizes and severities, and vegetation regrowth under various aridity conditions. The WildfireGenerator test results show different fire-vegetation recovery feedbacks related to the aridity conditions. Under low aridity, vegetation evolves almost to a homogeneous spatial distribution within the landscape due to high moisture, fast vegetation recovery, and low fire activity. Under intermediate aridity, fire frequency is at its peak, vegetation gets less dense, but is still well connected due to efficient post-fire regrowth rates. Under high aridity, vegetation is scarce and is not well connected, resulting in the highest soil exposure of all scenarios. The fires produced by WildfireGenerator replicate the frequency-magnitude distribution of observed fires, indicating that our simulations of fire activity are realistic. We tested FireLands coupled fire-erosion model by simulating the impact of fires on synthetically evolving topography. In FireLands, after a fire, there is a tendency for sediment to be transported from hillslopes to river channels. Variations in sediment redistribution and evacuation are mainly controlled by the balance between fire severity, vegetation recovery rates, and the presence of fire breaking rivers. FireLands is implemented in the Landlab framework, thereby

https://doi.org/10.5194/egusphere-2026-3521
Preprint. Discussion started: 3 August 2026

facilitating the use of *WildfireGenerator* component with various already available (and potentially new) geomorphic transport models. The current version of FireLands is suitable for assessing the large-scale impact of cumulative fire activity on evolving landscapes and for addressing the impact of various fire regimes on soil supply and fire-related erosion. The primary advantage of FireLands is its capacity to simulate the effects of fire-vegetation feedbacks on sediment transport over greater spatial and temporal scales than previous modeling works (e.g. Vieira et al., 2026). FireLands is a useful tool to apply on fire-prone landscapes facing rapid environmental changes, as changing fire regimes due to climate variations may have a large impact on sediment redistribution.

Code availability. The static version of the Landlab software package including the components and tutorial notebooks developed for the FireLands model is archived at: https://doi.org/10.5281/zenodo.21121799 (de Almeida, 2026). For FireLands installation, the user should clone the static version of Landlab with WildfireGenerator component included, install using ‘pip install -e‘, and run the tutorial notebooks under "/source/tutorials/wildfires/FireLands_tutorial.ipynb". FireLands code is also available at https://github.com/landlab/landlab/pull/2429, where code comments can be posted. Note that WildfireGenerator is currently under review as a pull request to the Landlab GitHub repository and is expected to be merged before the resubmission of this manuscript. Landlab’s documentation, including installation instructions and software dependencies can be found at: https://landlab.csdms.io/ (last access: June 2026).

Author contributions. MA, BC, CMS, DCRB conceptualized the model. BC and DCRB developed the project idea. MA developed the model code with help from BC. MA designed and performed the simulations, wrote the original draft and prepared the manuscript with contributions from all co-authors.

Competing interests. The authors declare that they have no conflict of interest.

Acknowledgements. This research was funded by the Dutch sectorgelden grant of BC and in part by the U.S. Department of Agriculture, Forest Service. The findings and conclusions in this publication are those of the authors and should not be construed to represent any official USDA or U.S. Government determination or policy. We thank Francis Rengers for reviewing an early draft of the paper.

https://doi.org/10.5194/egusphere-2026-3521
Preprint. Discussion started: 3 August 2026

References

Abrahams, E. R., Kaste, J. M., Ouimet, W., and Dethier, D. P.: Asymmetric hillslope erosion following wildfire in Fourmile Canyon, Colorado, Earth Surface Processes and Landforms, 43, 2009–2021, https://doi.org/10.1002/esp.4348, 2018.

Abram, N. J., Henley, B. J., Sen Gupta, A., Lippmann, T. J. R., Clarke, H., Dowdy, A. J., Sharples, J. J., Nolan, R. H., Zhang, T., Wooster, M. J., Wurtzel, J. B., Meissner, K. J., Pitman, A. J., Ukkola, A. M., Murphy, B. P., Tapper, N. J., and Boer, M. M.: Connections of climate change and variability to large and extreme forest fires in southeast Australia, Communications Earth & Environment, 2, 8, https://doi.org/10.1038/s43247-020-00065-8, 2021.

Alessio, P., Dunne, T., and Morell, K.: Post-Wildfire Generation of Debris-Flow Slurry by Rill Erosion on Colluvial Hillslopes, Journal of Geophysical Research: Earth Surface, 126, https://doi.org/10.1029/2021JF006108, 2021.

Anderson, D. B.: Relative Humidity or Vapor Pressure Deficit, Ecology, 17, 277–282, https://doi.org/10.2307/1931468, _eprint: https://esajournals.onlinelibrary.wiley.com/doi/pdf/10.2307/1931468, 1936.

Anderson, R. S.: Modeling the tor-dotted crests, bedrock edges, and parabolic profiles of high alpine surfaces of the Wind River Range, Wyoming, Geomorphology, 46, 35–58, https://doi.org/10.1016/S0169-555X(02)00053-3, 2002.

Archibald, S., Roy, D. P., Van WILGEN, B. W., and Scholes, R. J.: What limits fire? An examination of drivers of burnt area in Southern Africa, Global Change Biology, 15, 613–630, https://doi.org/10.1111/j.1365-2486.2008.01754.x, _eprint: https://onlinelibrary.wiley.com/doi/pdf/10.1111/j.1365-2486.2008.01754.x, 2009.

Ariagno, C., Le Bouteiller, C., Campforts, B., van der Beek, P., and Tucker, G.: Modeling Seasonal Sediment Dynamics and Landscape Evolution in a Marly Badland Catchment, Draix-Bléone Critical Zone Observatory, SE France, Journal of Geophysical Research: Earth Surface, 130, e2024JF008 183, https://doi.org/10.1029/2024JF008183, _eprint: https://agupubs.onlinelibrary.wiley.com/doi/pdf/10.1029/2024JF008183, 2025.

Barnhart, K. R., Glade, R. C., Shobe, C. M., and Tucker, G. E.: Terrainbento 1.0: a Python package for multi-model analysis in long-term drainage basin evolution, Geoscientific Model Development, 12, 1267–1297, https://doi.org/10.5194/gmd-12-1267-2019, 2019.

Barnhart, K. R., Hutton, E. W. H., Tucker, G. E., Gasparini, N. M., Istanbulluoglu, E., Hobley, D. E. J., Lyons, N. J., Mouchene, M., Nudurupati, S. S., Adams, J. M., and Bandaragoda, C.: Short communication: Landlab v2.0: a software package for Earth surface dynamics, Earth Surface Dynamics, 8, 379–397, https://doi.org/10.5194/esurf-8-379-2020, 2020.

Barrett, C. M., Kelly, R., Higuera, P. E., and Hu, F. S.: Climatic and land cover influences on the spatiotemporal dynamics of Holocene boreal fire regimes, Ecology, 94, 389–402, https://doi.org/10.1890/12-0840.1, _eprint: https://esajournals.onlinelibrary.wiley.com/doi/pdf/10.1890/12-0840.1, 2013.

Benavides-Solorio, J. and MacDonald, L.: Measurement and prediction of post-fire erosion at the hillslope scale, Colorado Front Range, International Journal of Wildland Fire, 14, 457–474, https://doi.org/10.1071/WF05042, 2005.

Benavides-Solorio, J. and MacDonald, L. H.: Post-fire runoff and erosion from simulated rainfall on small plots, Colorado Front Range, Hydrological Processes, 15, 2931–2952, https://doi.org/10.1002/hyp.383, _eprint: https://onlinelibrary.wiley.com/doi/pdf/10.1002/hyp.383, 2001.

Bircher, P., Liniger, H. P., and Prasuhn, V.: Comparison of long-term field-measured and RUSLE-based modelled soil loss in Switzerland, Geoderma Regional, 31, e00 595, https://doi.org/10.1016/j.geodrs.2022.e00595, 2022.

https://doi.org/10.5194/egusphere-2026-3521
Preprint. Discussion started: 3 August 2026

Bradstock, R. A.: A biogeographic model of fire regimes in Australia: current and future implications, Global Ecology and Biogeography, 19, 145–158, https://doi.org/10.1111/j.1466-8238.2009.00512.x, _eprint: https://onlinelibrary.wiley.com/doi/pdf/10.1111/j.1466-8238.2009.00512.x, 2010.

Campforts, B., Shobe, C. M., Steer, P., Vanmaercke, M., Lague, D., and Braun, J.: HyLands 1.0: a hybrid landscape evolution model to simulate the impact of landslides and landslide-derived sediment on landscape evolution, Geoscientific Model Development, 13, 3863–3886, https://doi.org/10.5194/gmd-13-3863-2020, 2020.

Campforts, B., Shobe, C. M., Overeem, I., and Tucker, G. E.: The Art of Landslides: How Stochastic Mass Wasting Shapes Topography and Influences Landscape Dynamics, Journal of Geophysical Research: Earth Surface, 127, e2022JF006 745, https://doi.org/10.1029/2022JF006745, _eprint: https://agupubs.onlinelibrary.wiley.com/doi/pdf/10.1029/2022JF006745, 2022.

Cardoso, A. W., Archibald, S., Bond, W. J., Coetsee, C., Forrest, M., Govender, N., Lehmann, D., Makaga, L., Mpanza, N., Ndong, J. E., Koumba Pambo, A. F., Strydom, T., Tilman, D., Wragg, P. D., and Staver, A. C.: Quantifying the environmental limits to fire spread in grassy ecosystems, Proceedings of the National Academy of Sciences, 119, e2110364 119, https://doi.org/10.1073/pnas.2110364119, 2022.

Cerdà, A.: Changes in overland flow and infiltration after a rangeland fire in a Mediterranean scrubland, Hydrological Processes, 12, 1031–1042, https://doi.org/10.1002/(SICI)1099-1085(19980615)12:7<1031::AID-HYP636>3.0.CO;2-V, 1998.

Chen, B., Jin, Y., Scaduto, E., Moritz, M. A., Goulden, M. L., and Randerson, J. T.: Climate, Fuel, and Land Use Shaped the Spatial Pattern of Wildfire in California's Sierra Nevada, Journal of Geophysical Research: Biogeosciences, 126, e2020JG005 786, https://doi.org/10.1029/2020JG005786, _eprint: https://agupubs.onlinelibrary.wiley.com/doi/pdf/10.1029/2020JG005786, 2021.

de Almeida, M.: FireLands 1.0: A landscape evolution model for simulating the effects of fires and post-fire erosion on sediment dynamics in evolving landscapes, https://doi.org/10.5281/zenodo.21121799, 2026.

DiBiase, R. A. and Lamb, M. P.: Dry sediment loading of headwater channels fuels post-wildfire debris flows in bedrock landscapes, Geology, 48, 189–193, https://doi.org/10.1130/g46847.1, 2019.

Dixon, J. L., Heimsath, A. M., Kaste, J., and Amundson, R.: Climate-driven processes of hillslope weathering, Geology, 37, 975–978, https://doi.org/10.1130/G30045A.1, 2009.

Doerr, S., Girona-Garcia, A., Sanchez, G. C., Badia-Villas, D., Bryant, R., Dickinson, M., Hsieh, R., Mataix-Solera, J., Miesel, J., Robichaud, P., Stoof, C. R., and Santín, C.: Soil heating during wildfires and prescribed burns: a global evaluation, INTERNATIONAL JOURNAL OF WILDLAND FIRE, https://doi.org/10.1071/WF25103, 2025.

Dow, H. W., East, A. E., Sankey, J. B., Warrick, J. A., Kostelnik, J., Lindsay, D. N., and Kean, J. W.: Postfire Sediment Mobilization and Its Downstream Implications Across California, 1984–2021, Journal of Geophysical Research: Earth Surface, 129, e2024JF007 725, https://doi.org/10.1029/2024JF007725, _eprint: https://agupubs.onlinelibrary.wiley.com/doi/pdf/10.1029/2024JF007725, 2024.

Finney, M. A.: An Overview of FlamMap Fire Modeling Capabilities, In: Andrews, Patricia L.; Butler, Bret W., comps. 2006. Fuels Management-How to Measure Success: Conference Proceedings. 28-30 March 2006; Portland, OR. Proceedings RMRS-P-41. Fort Collins, CO: U.S. Department of Agriculture, Forest Service, Rocky Mountain Research Station. p. 213-220, 041, https://research.fs.usda.gov/treesearch/25948, 2006.

Flanagan, D. C. and Nearing, M. A.: USDA - Water Erosion Prediction Project Hillslope Profile and Watershed Model Documentation, Tech. Rep. NSERL Report No. 10, USDA-ARS National Soil Erosion Research Laboratory, 1995.

Freire, J. G. and DaCamara, C. C.: Using cellular automata to simulate wildfire propagation and to assist in fire prevention and fighting, https://doi.org/10.5194/nhess-2018-227, 2018.

https://doi.org/10.5194/egusphere-2026-3521
Preprint. Discussion started: 3 August 2026

Ganti, V., Passalacqua, P., and Foufoula-Georgiou, E.: A sub-grid scale closure for nonlinear hillslope sediment transport models, Journal of Geophysical Research: Earth Surface, 117, https://doi.org/10.1029/2011JF002181, _eprint: https://agupubs.onlinelibrary.wiley.com/doi/pdf/10.1029/2011JF002181, 2012.

Geyman, E. C., Paige, D. A., and Lamb, M. P.: The contribution of rock strength to soil production, Nature, 647, 921–927, https://doi.org/10.1038/s41586-025-09751-z, 2025.

Gouveia, C., DaCamara, C. C., and Trigo, R. M.: Post-fire vegetation recovery in Portugal based on spot/vegetation data, Natural Hazards and Earth System Sciences, 10, 673–684, https://doi.org/10.5194/nhess-10-673-2010, 2010.

Grünig, M., Seidl, R., and Senf, C.: Increasing aridity causes larger and more severe forest fires across Europe, Global Change Biology, 29, 1648–1659, https://doi.org/10.1111/gcb.16547, _eprint: https://onlinelibrary.wiley.com/doi/pdf/10.1111/gcb.16547, 2023.

Guilinger, J. J., Foufoula-Georgiou, E., Gray, A. B., Randerson, J. T., Smyth, P., Barth, N. C., and Goulden, M. L.: Predicting Postfire Sediment Yields of Small Steep Catchments Using Airborne Lidar Differencing, Geophysical Research Letters, 50, e2023GL104 626, https://doi.org/10.1029/2023GL104626, _eprint: https://agupubs.onlinelibrary.wiley.com/doi/pdf/10.1029/2023GL104626, 2023.

Hantson, S., Arneth, A., Harrison, S. P., Kelley, D. I., Prentice, I. C., Rabin, S. S., Archibald, S., Mouillot, F., Arnold, S. R., Artaxo, P., Bachelet, D., Ciais, P., Forrest, M., Friedlingstein, P., Hickler, T., Kaplan, J. O., Kloster, S., Knorr, W., Lasslop, G., Li, F., Mangeon, S., Melton, J. R., Meyn, A., Sitch, S., Spessa, A., van der Werf, G. R., Voulgarakis, A., and Yue, C.: The status and challenge of global fire modelling, Biogeosciences, 13, 3359–3375, https://doi.org/10.5194/bg-13-3359-2016, 2016.

Heimsath, A., Dietrich, W., Nishiizumi, K., and Finkel, R.: The Soil Production Function and Landscape Equilibrium, Nature, 388, https://doi.org/10.1038/41056, 1997.

Hobley, D. E. J., Adams, J. M., Nudurupati, S. S., Hutton, E. W. H., Gasparini, N. M., Istanbulluoglu, E., and Tucker, G. E.: Creative computing with Landlab: an open-source toolkit for building, coupling, and exploring two-dimensional numerical models of Earth-surface dynamics, Earth Surface Dynamics, 5, 21–46, https://doi.org/10.5194/esurf-5-21-2017, 2017.

Inbar, M., Tamir, M., and Wittenberg, L.: Runoff and erosion processes after a forest fire in Mount Carmel, a Mediterranean area, Geomorphology, 24, 17–33, https://doi.org/10.1016/S0169-555X(97)00098-6, 1998.

Istanbulluoglu, E. and Bras, R. L.: Vegetation-modulated landscape evolution: Effects of vegetation on landscape processes, drainage density, and topography, Journal of Geophysical Research: Earth Surface, 110, https://doi.org/10.1029/2004JF000249, _eprint: https://agupubs.onlinelibrary.wiley.com/doi/pdf/10.1029/2004JF000249, 2005.

Jackson, M. and Roering, J. J.: Post-fire geomorphic response in steep, forested landscapes: Oregon Coast Range, USA, Quaternary Science Reviews, 28, 1131–1146, https://doi.org/10.1016/j.quascirev.2008.05.003, 2009.

Kampf, S. K., Stevens-Rumann, C. S., Nunes, L., Sequeira, A. C., Rego, F. C., Fernández, C., Hernández-Duarte, A., Mosso, C. E., Francois, J. P., and Miranda, A.: Fire, Fuel, and Climate Interactions in Temperate Climates, AGU Advances, 6, e2024AV001 628, https://doi.org/10.1029/2024AV001628, _eprint: https://agupubs.onlinelibrary.wiley.com/doi/pdf/10.1029/2024AV001628, 2025.

Karamesouti, M., Petropoulos, G. P., Papanikolaou, I. D., Kairis, O., and Kosmas, K.: Erosion rate predictions from PESERA and RUSLE at a Mediterranean site before and after a wildfire: Comparison & implications, Geoderma, 261, 44–58, https://doi.org/10.1016/j.geoderma.2015.06.025, 2016.

Kinnell, P.: Raindrop-impact-induced erosion processes and prediction: A review, Hydrological Processes, 19, 2815–2844, https://doi.org/10.1002/hyp.5788, 2005.

Kirkby, M. J., Irvine, B. J., Jones, R. J. A., Govers, G., and Team, P.: The PESERA coarse scale erosion model for Europe. I. – Model rationale and implementation, European Journal of Soil Science, 59, 1293–1306, https://doi.org/10.1111/j.1365-2389.2008.01072.x, _eprint: https://bsssjournals.onlinelibrary.wiley.com/doi/pdf/10.1111/j.1365-2389.2008.01072.x, 2008.

Krawchuk, M. A. and Moritz, M. A.: Constraints on global fire activity vary across a resource gradient, Ecology, 92, 121–132, https://doi.org/10.1890/09-1843.1, _eprint: https://esajournals.onlinelibrary.wiley.com/doi/pdf/10.1890/09-1843.1, 2011.

Lamb, M. P., Scheingross, J. S., Amidon, W. H., Swanson, E., and Limaye, A.: A model for fire-induced sediment yield by dry ravel in steep landscapes, Journal of Geophysical Research: Earth Surface, 116, https://doi.org/10.1029/2010JF001878, _eprint: https://agupubs.onlinelibrary.wiley.com/doi/pdf/10.1029/2010JF001878, 2011.

Larsen, I. J. and MacDonald, L. H.: Predicting postfire sediment yields at the hillslope scale: Testing RUSLE and Disturbed WEPP, Water Resources Research, 43, https://doi.org/10.1029/2006WR005560, _eprint: https://agupubs.onlinelibrary.wiley.com/doi/pdf/10.1029/2006WR005560, 2007.

Larsen, I. J., MacDonald, L. H., Brown, E., Rough, D., Welsh, M. J., Pietraszek, J. H., Libohova, Z., de Dios Benavides-Solorio, J., and Schaffrath, K.: Causes of Post-Fire Runoff and Erosion: Water Repellency, Cover, or Soil Sealing?, Soil Science Society of America Journal, 73, 1393–1407, https://doi.org/10.2136/sssaj2007.0432, _eprint: https://acsess.onlinelibrary.wiley.com/doi/pdf/10.2136/sssaj2007.0432, 2009.

Liu, N., Chen, H., Xie, X., Zhang, L., Yao, B., Zhu, J., and Shan, Y.: Effect of slope on spread of a linear flame front over a pine needle fuel bed: experiments and modelling, International Journal of Wildland Fire, 23, 1087–1096, https://doi.org/10.1071/WF12189, 2014.

McGuire, L. A., Ebel, B. A., Rengers, F. K., Vieira, D. C. S., and Nyman, P.: Fire effects on geomorphic processes, Nature Reviews Earth & Environment, 5, 486–503, https://doi.org/10.1038/s43017-024-00557-7, 2024.

Moody, J. A., Shakesby, R. A., Robichaud, P. R., Cannon, S. H., and Martin, D. A.: Current research issues related to post-wildfire runoff and erosion processes, Earth-Science Reviews, 122, 10–37, https://doi.org/10.1016/j.earscirev.2013.03.004, 2013.

Morgan, P., Hardy, C. C., Swetnam, T. W., Rollins, M. G., and Long, D. G.: Mapping fire regimes across time and space: Understanding coarse and fine-scale fire patterns, International Journal of Wildland Fire, 10, 329–342, https://doi.org/10.1071/WF01032, 2001.

Moritz, M. A., Morais, M. E., Summerell, L. A., Carlson, J. M., and Doyle, J.: Wildfires, complexity, and highly optimized tolerance, Proceedings of the National Academy of Sciences, 102, 17 912–17 917, https://doi.org/10.1073/pnas.0508985102, 2005.

Noske, P. J., Nyman, P., Lane, P. N. J., and Sheridan, G. J.: Effects of aridity in controlling the magnitude of runoff and erosion after wildfire, Water Resources Research, 52, 4338–4357, https://doi.org/10.1002/2015WR017611, _eprint: https://agupubs.onlinelibrary.wiley.com/doi/pdf/10.1002/2015WR017611, 2016.

Noske, P. J., Nyman, P., Lane, P. N. J., Rengers, F. K., and Sheridan, G. J.: Changes in soil erosion caused by wildfire: A conceptual biogeographic model, Geomorphology, 459, 109 272, https://doi.org/10.1016/j.geomorph.2024.109272, 2024.

Nudurupati, S. S., Istanbulluoglu, E., Tucker, G. E., Gasparini, N. M., Hobley, D. E. J., Hutton, E. W. H., Barnhart, K. R., and Adams, J. M.: On Transient Semi-Arid Ecosystem Dynamics Using Landlab: Vegetation Shifts, Topographic Refugia, and Response to Climate, Water Resources Research, 59, e2021WR031 179, https://doi.org/10.1029/2021WR031179, _eprint: https://agupubs.onlinelibrary.wiley.com/doi/pdf/10.1029/2021WR031179, 2023.

Nyman, P., Sheridan, G. J., Moody, J. A., Smith, H. G., Noske, P. J., and Lane, P. N. J.: Sediment availability on burned hillslopes, Journal of Geophysical Research: Earth Surface, 118, 2451–2467, https://doi.org/10.1002/jgrf.20152, _eprint: https://agupubs.onlinelibrary.wiley.com/doi/pdf/10.1002/jgrf.20152, 2013.

https://doi.org/10.5194/egusphere-2026-3521
Preprint. Discussion started: 3 August 2026

Orem, C. A. and Pelletier, J. D.: The predominance of post-wildfire erosion in the long-term denudation of the Valles Caldera, New Mexico, Journal of Geophysical Research: Earth Surface, 121, 843–864, https://doi.org/10.1002/2015JF003663, _eprint: https://agupubs.onlinelibrary.wiley.com/doi/pdf/10.1002/2015JF003663, 2016.

Pais, C., Carrasco, J., Martell, D. L., Weintraub, A., and Woodruff, D. L.: Cell2Fire: A Cell-Based Forest Fire Growth Model to Support Strategic Landscape Management Planning, Frontiers in Forests and Global Change, 4, https://doi.org/10.3389/ffgc.2021.692706, 2021.

Parks, S. A., Coop, J. D., and Davis, K. T.: Intensifying Fire Season Aridity Portends Ongoing Expansion of Severe Wildfire in Western US Forests, Glob Chang Biol, 31, e70 429, https://doi.org/10.1111/gcb.70429, 2025.

Pausas, J. G. and Bradstock, R. A.: Fire persistence traits of plants along a productivity and disturbance gradient in mediterranean shrublands of south-east Australia, Global Ecology and Biogeography, 16, 330–340, https://doi.org/10.1111/j.1466-8238.2006.00283.x, _eprint: https://onlinelibrary.wiley.com/doi/pdf/10.1111/j.1466-8238.2006.00283.x, 2007.

Pausas, J. G. and Paula, S.: Fuel shapes the fire–climate relationship: evidence from Mediterranean ecosystems, Global Ecology and Biogeography, 21, 1074–1082, https://doi.org/10.1111/j.1466-8238.2012.00769.x, _eprint: https://onlinelibrary.wiley.com/doi/pdf/10.1111/j.1466-8238.2012.00769.x, 2012.

Pausas, J. G. and Ribeiro, E.: The global fire–productivity relationship, Global Ecology and Biogeography, 22, 728–736, https://doi.org/10.1111/geb.12043, _eprint: https://onlinelibrary.wiley.com/doi/pdf/10.1111/geb.12043, 2013.

Perron, J. T.: Numerical methods for nonlinear hillslope transport laws, Journal of Geophysical Research: Earth Surface, 116, https://doi.org/10.1029/2010JF001801, _eprint: https://agupubs.onlinelibrary.wiley.com/doi/pdf/10.1029/2010JF001801, 2011.

Ren, Y., Zhang, Y., Yuan, X., Pan, B., Zhang, Q., and Geng, H.: A Modular Implicit Numerical Method for Hillslope Sediment Transport Laws, Journal of Geophysical Research: Earth Surface, 131, e2025JF008 675, https://doi.org/10.1029/2025JF008675, 2026.

Renard, K. G., Foster, G. R., and Weesies, G. A.: Revised universal soil loss equation, Journal of Soil and Water Conservation, 1991.

Rengers, F. and Mcguire, L.: Wildfire and earth surface processes, Earth Surface Processes and Landforms, 46, 1099–1102, https://doi.org/10.1002/esp.5054, 2021.

Rengers, F. K., Tucker, G. E., Moody, J. A., and Ebel, B. A.: Illuminating wildfire erosion and deposition patterns with repeat terrestrial lidar, Journal of Geophysical Research: Earth Surface, 121, 588–608, https://doi.org/10.1002/2015JF003600, _eprint: https://agupubs.onlinelibrary.wiley.com/doi/pdf/10.1002/2015JF003600, 2016.

Rengers, F. K., McGuire, L. A., Kean, J. W., Staley, D. M., Dobre, M., Robichaud, P. R., and Swetnam, T.: Movement of Sediment Through a Burned Landscape: Sediment Volume Observations and Model Comparisons in the San Gabriel Mountains, California, USA, Journal of Geophysical Research: Earth Surface, 126, e2020JF006 053, https://doi.org/10.1029/2020JF006053, _eprint: https://agupubs.onlinelibrary.wiley.com/doi/pdf/10.1029/2020JF006053, 2021.

Rengers, F. K., Stoker, J. M., Kostelnik, J., Kean, J. W., Wohl, E. E., Barnhart, K. R., and Guido, L. E.: Channel morphology and large wood control postfire debris-flow erosion and deposition, Earth Surface Processes and Landforms, 51, e70 287, https://doi.org/10.1002/esp.70287, _eprint: https://onlinelibrary.wiley.com/doi/pdf/10.1002/esp.70287, 2026.

Rice, R. M.: Sedimentation in the Chaparral: How Do You Handle Unusual Events?, in: Workshop on sediment budgets and routing in forested drainage basins: proceedings., edited by Swanston, F. J., vol. 141 of *Gen. Tech. Rep. PNW-GTR-141. Portland, OR: U.S. Department of Agriculture, Forest Service, Pacific Northwest Research Station. 165 p*, pp. 39–49, https://doi.org/https://doi.org/10.2737/PNW-GTR-141, 1982.

Roering, J. J. and Gerber, M.: Fire and the evolution of steep, soil-mantled landscapes, Geology, 33, 349–352, https://doi.org/10.1130/G21260.1, 2005.

https://doi.org/10.5194/egusphere-2026-3521
Preprint. Discussion started: 3 August 2026

Rothermel, R. C.: A mathematical model for predicting fire spread in wildland fuels, Res. Pap. INT-115. Ogden, UT: U.S. Department of Agriculture, Intermountain Forest and Range Experiment Station. 40 p., 115, https://research.fs.usda.gov/treesearch/32533, 1972.

Ryan, S. E., Shobe, C. M., Rathburn, S. L., and Dixon, M. K.: Suspended-sediment response to wildfire and a major post-fire flood on the Colorado Front Range, River Research and Applications, 40, 1256–1272, https://doi.org/10.1002/rra.4286, 2024.

San-Miguel-Ayanz, J., Schulte, E., Schmuck, G., Camia, A., Strobl, P., Libertà, G., Giovando, C., Boca, R., Sedano, F., Kempeneers, P., McInerney, D., Withmore, C., Oliveira, S., Rodrigues, M., Durrant, T., Corti, P., Oehler, F., Vilar, L., and Amatulli, G.: Comprehensive Monitoring of Wildfires in Europe: The European Forest Fire Information System (EFFIS), in: Approaches to Managing Disaster - Assessing Hazards, Emergencies and Disaster Impacts, https://doi.org/10.5772/28441, journal Abbreviation: Approaches to Managing Disaster - Assessing Hazards, Emergencies and Disaster Impacts, 2012.

Sanginés de Cárcer, P., Vitasse, Y., Peñuelas, J., Jassey, V. E. J., Buttler, A., and Signarbieux, C.: Vapor–pressure deficit and extreme climatic variables limit tree growth, Global Change Biology, 24, 1108–1122, https://doi.org/10.1111/gcb.13973, _eprint: https://onlinelibrary.wiley.com/doi/pdf/10.1111/gcb.13973, 2018.

Santi, P. and Rengers, F.: Wildfire and Landscape Change, in: Reference Module in Earth Systems and Environmental Sciences, https://doi.org/10.1016/B978-0-12-818234-5.00017-1, journal Abbreviation: Reference Module in Earth Systems and Environmental Sciences, 2020.

Scholten, R. C., Veraverbeke, S., Chen, Y., and Randerson, J. T.: Spatial variability in Arctic–boreal fire regimes influenced by environmental and human factors, Nature Geoscience, 17, 866–873, https://doi.org/10.1038/s41561-024-01505-2, 2024.

Sedano, F. and Randerson, J. T.: Multi-scale influence of vapor pressure deficit on fire ignition and spread in boreal forest ecosystems, Biogeosciences, 11, 3739–3755, https://doi.org/10.5194/bg-11-3739-2014, 2014.

Shakesby, R. A. and Doerr, S. H.: Wildfire as a hydrological and geomorphological agent, Earth-Science Reviews, 74, 269–307, https://doi.org/10.1016/j.earscirev.2005.10.006, 2006.

Shmilovitz, Y., Rossi, M. W., and Tucker, G. E.: Multi-Century Erosion and Landscape Evolution of Ephemeral Catchments in Response to Sub-Daily Rainfall Distribution Changes, Geophysical Research Letters, 52, e2024GL113 179, https://doi.org/10.1029/2024GL113179, _eprint: https://agupubs.onlinelibrary.wiley.com/doi/pdf/10.1029/2024GL113179, 2025.

Shobe, C. M., Tucker, G. E., and Barnhart, K. R.: The SPACE 1.0 model: a Landlab component for 2-D calculation of sediment transport, bedrock erosion, and landscape evolution, Geoscientific Model Development, 10, 4577–4604, https://doi.org/10.5194/gmd-10-4577-2017, 2017.

Sousa, D. F. M., Fulmer, E., Sanders, M. A., Mathews, N. W., Roering, J. J., Rengers, F. K., Mirus, B. B., Burns, W. J., Olsen, M. J., and Leshchinsky, B. A.: The influence of postfire root strength decay on shallow landslide susceptibility in western Oregon, Landslides, 23, 1–18, https://doi.org/10.1007/s10346-025-02643-3, 2026.

Tarquini, S., Isola, I., Favalli, M., Mazzarini, F., Bisson, M., Pareschi, M. T., and Boschi, E.: TINITALY/01: a new Triangular Irregular Network of Italy, Annals of Geophysics, 50, 407–425, https://doi.org/10.4401/ag-4424, 2007.

Thomas, M. A., Lindsay, D. N., Kean, J. W., Graber, A. P., Rossi, R. K., Kostelnik, J., Rengers, F. K., Schwartz, J. Y., Swanson, B. J., Oakley, N. S., Richardson, P. W., Morelan, A. E., Ritchie, A. C., Warrick, J. A., Rotche, L. L., Penserini, B. D., and Slaughter, S. L.: Landsliding follows signatures of wildfire history and vegetation regrowth in a steep coastal shrubland, Geosphere, 21, 823–840, https://doi.org/10.1130/GES02856.1, 2025.

Toffoli, T.: Cellular automata as an alternative to (rather than an approximation of) differential equations in modeling physics, Physica D: Nonlinear Phenomena, 10, 117–127, https://doi.org/10.1016/0167-2789(84)90254-9, 1984.

https://doi.org/10.5194/egusphere-2026-3521
Preprint. Discussion started: 3 August 2026

Tucker, G. E. and Hancock, G. R.: Modelling landscape evolution, Earth Surface Processes and Landforms, 35, 28–50, https://doi.org/10.1002/esp.1952, _eprint: https://onlinelibrary.wiley.com/doi/pdf/10.1002/esp.1952, 2010.

Veraverbeke, S., Lhermitte, S., Verstraeten, W. W., and Goossens, R.: The temporal dimension of differenced Normalized Burn Ratio (dNBR) fire/burn severity studies: The case of the large 2007 Peloponnese wildfires in Greece, Remote Sensing of Environment, 114, 2548–2563, https://doi.org/10.1016/j.rse.2010.05.029, 2010.

Viedma, O., Meliá, J., Segarra, D., and Garcia-Haro, J.: Modeling rates of ecosystem recovery after fires by using landsat TM data, Remote Sensing of Environment, 61, 383–398, https://doi.org/10.1016/S0034-4257(97)00048-5, 1997.

Vieira, D. C. S., Malvar, M. C., Martins, M. A. S., Serpa, D., and Keizer, J. J.: Key factors controlling the post-fire hydrological and erosive response at micro-plot scale in a recently burned Mediterranean forest, Geomorphology, 319, 161–173, https://doi.org/10.1016/j.geomorph.2018.07.014, 2018.

Vieira, D. C. S., Borrelli, P., Jahanianfard, D., Benali, A., Scarpa, S., and Panagos, P.: Wildfires in Europe: Burned soils require attention, Environ Res, 217, 114 936, https://doi.org/10.1016/j.envres.2022.114936, 2023.

Vieira, D. C. S., Borrelli, P., Scarpa, S., Liakos, L., Ballabio, C., and Panagos, P.: Global estimation of post-fire soil erosion, Nature Geoscience, 19, 59–67, https://doi.org/10.1038/s41561-025-01876-0, 2026.

Wolfram, S.: Cellular automata and complexity: collected papers, vol. 1, Westview Press, Boulder, CO, 1994.

Yuan, W., Zheng, Y., Piao, S., Ciais, P., Lombardozzi, D., Wang, Y., Ryu, Y., Chen, G., Dong, W., Hu, Z., Jain, A. K., Jiang, C., Kato, E., Li, S., Lienert, S., Liu, S., Nabel, J. E., Qin, Z., Quine, T., Sitch, S., Smith, W. K., Wang, F., Wu, C., Xiao, Z., and Yang, S.: Increased atmospheric vapor pressure deficit reduces global vegetation growth, Science Advances, 5, eaax1396, https://doi.org/10.1126/sciadv.aax1396, 2019.

Zhou, Z., Xu, Q., Yi, J., Li, Y., Zhang, S., and Li, W.: Modeling the spread of forest fires through cellular automata by leveraging deep learning to derive transition rules, Ecological Informatics, 88, 103 150, https://doi.org/10.1016/j.ecoinf.2025.103150, 2025.